ADVANCED FUNCTIONAL MATERIALS
www.afm-journal.de

Wearable and Implantable Devices for Cardiovascular Healthcare: from Monitoring to Therapy Based on Flexible and Stretchable Electronics

Yongseok Joseph Hong, Hyoyoung Jeong, Kyoung Won Cho, Nanshu Lu, and Dae-Hyeong Kim**

Cardiovascular disease is the leading cause of death and has dramatically increased in recent years. Continuous cardiac monitoring is particularly important for early diagnosis and prevention, and flexible and stretchable electronic devices have emerged as effective tools for this purpose. Their thin, soft, and deformable features allow intimate and long-term integration with biotissues, which enables continuous, high-fidelity, and sometimes large-area cardiac monitoring on the skin and/or heart surface. In addition to monitoring, intimate contact is also crucial for high-precision therapies. Combined with tissue engineering, soft bioelectronics have also demonstrated the capability to repair damaged cardiac tissues. This review highlights the recent advances in wearable and implantable devices based on flexible and stretchable electronics for cardiovascular monitoring and therapy. First, wearable/implantable soft bioelectronics for cardiovascular monitoring (e.g., the electrocardiogram, blood pressure, and oxygen saturation level) are reviewed. Then, advances in cardiovascular therapy based on soft bioelectronics (e.g., mesh pacing, ablation, robotic sleeves, and electronic stents) are discussed. Finally, device-assisted tissue engineering therapy (e.g., functional electronic scaffolds and in vitro cardiac platforms) is discussed.

1. Introduction

The heart is a vital organ that pumps blood through blood vessels to provide oxygen (O_2) and nutrients throughout the entire body and to remove carbon dioxide (CO_2) and metabolic waste from the body. The World Health Organization estimated that cardiovascular diseases (CVDs), i.e., heart and blood vessel diseases, are responsible for up to ≈30% of the total number of deaths worldwide.[1,2] Since CVDs become much easier to manage when detected early, there is an increasing need for continuous cardiovascular monitoring.[3,4] For example, various CVDs can be indicated by interpreting the patterns of electrocardiograms (ECGs).[5–8] Meanwhile, monitoring the blood pressure (BP) and blood oxygen saturation is also common practice. This is because an elevated BP is one of the most important risk factors in cardiovascular morbidity,[9] and a low baseline for the blood oxygen saturation level is useful in the diagnosis of acute heart failure. When abnormal heart rhythms or heart failure is detected, timely and accurate treatment is vital. As a result, there are significant needs for the research and development of cardiovascular monitoring and therapeutic devices, which have to be enabled by novel material and design innovations.

Rapid advances in flexible and stretchable electronics[10–12] have enabled the development of soft wearable (**Figure 1**a) and implantable (Figure 1b) devices.[13–17] By utilizing ultrathin and soft materials,[18–22] soft bioelectronic devices can reliably and unobstructively interface with parts of human body,[23,24] such as the skin and/or internal organs including the heart, to monitor human physiological signals with a high fidelity.[25–28] In particular, for electrophysiological signals, conformal device–tissue contact can effectively reduce the electrode–skin interface impedance and mechanical sliding, minimizing motion artifacts. Some of these devices are so soft that they can fully wrap around the heart and blood vessels in 3D space without imposing any mechanical deformation to the soft tissue or causing any mechanical constraint on the natural motion of the heart. Compared with conventional lead-like cardiac implants, 3D integumentary membranes have enabled unprecedented

Y. J. Hong, K. W. Cho, Prof. D.-H. Kim
Center for Nanoparticle Research
Institute for Basic Science (IBS)
Seoul 08826, Republic of Korea
E-mail: dkim98@snu.ac.kr
Y. J. Hong, K. W. Cho, Prof. D.-H. Kim
School of Chemical and Biological Engineering
Institute of Chemical Processes
Seoul National University (SNU)
Seoul 08826, Republic of Korea
H. Jeong
Department of Electrical and Computer Engineering
University of Texas at Austin
Austin, TX 78712, USA
Prof. N. Lu
Department of Aerospace Engineering and Engineering Mechanics
University of Texas at Austin
Austin, TX 78712, USA
E-mail: nanshulu@utexas.edu
The ORCID identification number(s) for the author(s) of this article can be found under https://doi.org/10.1002/adfm.201808247.

DOI: 10.1002/adfm.201808247

functions such as 3D high-resolution spatiotemporal mapping of the entire heart. Furthermore, the integration of wireless communication units avoids the use of messy wires, and enables continuous cardiac health monitoring with mobility, which represents a major advancement toward ambulatory monitoring.

In addition to cardiac monitoring devices, flexible and stretchable bioelectronics have also been applied for improved in vivo cardiovascular therapies (Figure 1c).[29] Conventional rigid medical implants are prone to inducing device-related complications such as local or systemic infection and inflammation. Electrical therapies confined within the small area corresponding to the electrode size show limited therapeutic efficacy. In contrast, soft treatment devices such as multifunctional integumentary membranes and inflatable balloon catheters utilize biocompatible materials to minimize device-related complications and are capable of carrying out large-area treatment of the epicardium or endocardium to effectively cure arrhythmia. Moreover, soft bioelectronics–based therapy can be supplemented by integrating device-assisted cell-based therapies, particularly for repairing the damaged cardiac tissues (Figure 1d).[16,30,31] Cells cultured in vitro under the appropriate environmental cues mimicking native conditions are prepared as a scaffold or cell sheet for implantation.[32,33] When integrated with soft bioelectronics, the efficacy of such tissue engineering therapeutics can be monitored in vivo.

In this review, we present the recent advances in soft bioelectronics especially designed for cardiac monitoring and therapy. The review starts by highlighting the advances in designs, materials, and structures for ECG electrodes, such as a filamentary serpentine (FS) design, 1D and 2D materials based composites, and bioinspired microstructures. Then, we scrutinize the wearable (i.e., ECG monitoring and pulse oximetry; Figure 1a) and implantable (BP monitoring and cardiac mapping; Figure 1b) soft bioelectronic devices especially developed for continuous cardiac monitoring. In addition, soft bioelectronics also enables more effective and controllable cardiac therapy (i.e., cardiac pacing, robotic sleeves, ablation therapy, and electronic stents; Figure 1c). Finally, cell-based therapies assisted by soft devices including functional electronic scaffolds and in vitro cardiac platforms are introduced with the possibility of realizing synergistic effects with soft bioelectronics–based therapies (Figure 1d). The application of flexible and stretchable electronics technology in cardiac devices has significantly improved the capability and quality of cardiac monitoring and therapy, and has provided many future opportunities for subsequent development.

Yongseok Joseph Hong received his B.S. (2016) degree from the School of Chemical and Biological Engineering at Seoul National University. Under the supervision of Prof. Dae-Hyeong Kim, he is working on the fabrication and application of stretchable electrochemical sensors and transdermal drug delivery systems.

Nanshu Lu received her B.S. (2005) degree from Tsinghua University, Beijing, and her Ph.D. (2009) degree from Harvard University. After two years of research as a Beckman postdoctoral fellow, she joined the Department of Aerospace Engineering and Engineering Mechanics at the University of Texas at Austin in 2011. She became tenured associate professor in 2017. Her research interest lies at the intersection of mechanics, materials, manufacture, and biointegration of soft electronics.

Dae-Hyeong Kim received his B.S. (2000) and M.S. (2002) degrees from the School of Chemical Engineering at Seoul National University. He obtained his Ph.D. (2009) degree from the Department of Materials Science and Engineering at the University of Illinois at Urbana-Champaign. Since he joined the faculty of the School of Chemical and Biological Engineering at Seoul National University in 2011, he has focused on stretchable electronics for biomedical and energy applications.

2. Soft Bioelectronics for Monitoring

2.1. Materials for Skin-Integrated Soft Electrodes

An ECG is the most essential and commonly used diagnostic tool for abnormal cardiac rhythms.[34] An ECG is induced from the electrical activity of the sinoatrial (SA) node and cardiac conduction system (CCS) of the heart, which can be measured invasively from the heart or epidermally. The depolarizing and repolarizing surface potential differences can be noninvasively measured through multi-lead electrodes located on the chest (Figure 1a, left) or limbs.[35] The quality of an ECG measured using surface electrodes is largely dependent upon the electrode–skin interface impedance and noise induced by motion.[36] Equivalent circuit models (i.e., parallel and series combinations of resistors and capacitors) are available to account for the complex structures and the characteristics of the skin layers in accordance with wet and dry electrodes.[36] Although electrodes with electrolytic gels are conventionally used for surface ECG recording, they are unfavored owing to their skin irritating and drying nature. Rigid dry electrodes are wearable long-term and reusable, but they suffer from a large electrode–skin impedance and motion artifacts. When the skin deforms, motion artifacts arise from electrode–skin sliding and

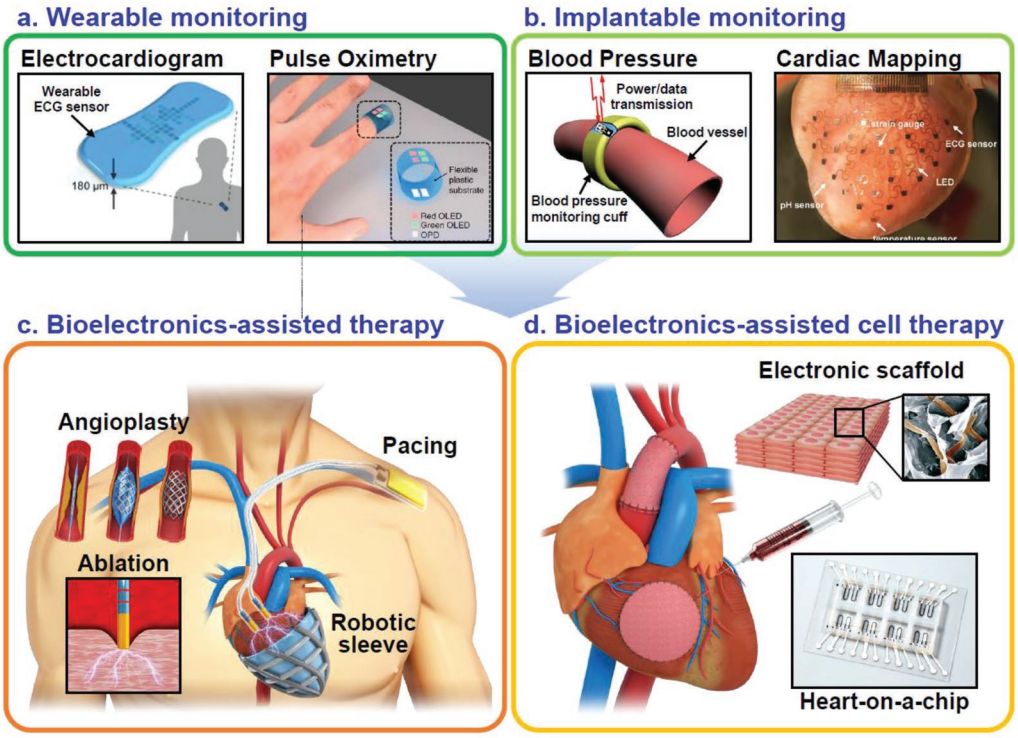

Figure 1. Overview of wearable and implantable devices for cardiovascular health management systems. a) Schematics of wearable monitoring devices including an ECG monitoring device (left) and pulse oximetry (right). Reproduced with permission.[35,73] Copyright 2018, Nature Publishing Group, Copyright 2014, Nature Publishing Group, respectively. b) Schematic and optical image of implantable monitoring devices including blood pressure monitoring (left) and cardiac mapping devices (right). Reproduced with permission.[91,96] Copyright 2009, IEEE, Copyright 2016, Wiley-VCH, respectively. c) Schematic of bioelectronics-assisted therapies including angioplasty (top left), pacing (top right), ablation therapy (bottom left), and a robotic sleeve (bottom right). d) Schematic of cardiac cell therapies (left) including a scaffold integrated with flexible and soft electronics (top right) and a heart-on-a-chip for providing native heart-like tissue and an in vitro environment (bottom right). Reproduced with permission.[296,309] Copyright 2012, Nature Publishing Group, Copyright 2016, Nature Publishing Group, respectively.

variations in the intrinsic skin impedance. Hence, soft stretchable electrodes have the obvious advantage of minimizing slippage against the skin by being able to deform with the skin without detachment or fracture. Numerous soft bioelectronics with advanced mechanics, materials, and design strategies have been reported for dry electrodes. The ultrathin and ultrasoft ones are able to fully conform to natural skin morphology and follow arbitrary skin deformation. Hence, they exhibit a low electrode–skin impedance and high signal-to-noise ratio (SNR), even under severe skin deformation.

Skin-conformable dry and soft surface electrodes originated from the idea of epidermal electronics (**Figure 2**a).[37] Au was the first choice of epidermal electrode materials because of its biocompatibility, chemical inertness, and suitable half-cell potential. A micrometer-thick Au bilayer on polyimide (PI) was first patterned into an FS mesh on a rigid wafer for handling and then transfer-printed onto a 30 μm thick skin-soft Ecoflex substrate backed by a water-soluble polyvinyl alcohol (PVA) substrate. To apply the Ecoflex-supported Au FS electrode to human skin, the PVA substrate can be dissolved by water, leaving the electrodes to self-conform to human skin via only van der Waals forces. As the thickness, Young's modulus, stretchability, and mass density of such electrodes can mimic the human epidermis well, they are called epidermal electrodes. Epidermal electrodes have been applied to successfully measure the surface ECG, electromyogram (EMG), electroencephalogram (EEG), and skin hydration, as indicated by the skin impedance.[37] A further development eliminated the Ecoflex substrate and directly printed the FS Au/PI electrodes onto the skin (Figure 2b).[38] Instead of Ecoflex, a biocompatible spray-on liquid bandage was applied over the FS electrodes to provide imperceptible but robust bonding to the skin. The first-generation epidermal electronics were manufactured through standard microelectronic fabrication processes,,[37–42] i.e., photolithography on rigid wafers that can be handled. Later, a dry and digital "cut-and-paste" manufacturing method was invented for the rapid prototyping of epidermal electronics.[43] This method utilizes a paper/vinyl cutter plotter to subtractively pattern bilayer Au/polyethylene terephthalate (PET) on a temporary supporting substrate, and the patterned FS mesh can be pasted onto any target substrate such as medical tape (e.g., Tegaderm) (Figure 2c). Compared with photolithographic processes, the "cut-and-paste" method is much more effective in terms of the fabrication cost, labor, and time. A major limitation of this method is that the patterning resolution of the cutter plotter is limited to 200 μm. Although some laser cutters can offer a higher patterning resolution, the thermal stress in and thermal damage to the thin films need to be carefully managed.[43–47] Recently, as a dry and digital freeform manufacturing method, laser patterning of printed circuit boards and electrodes has

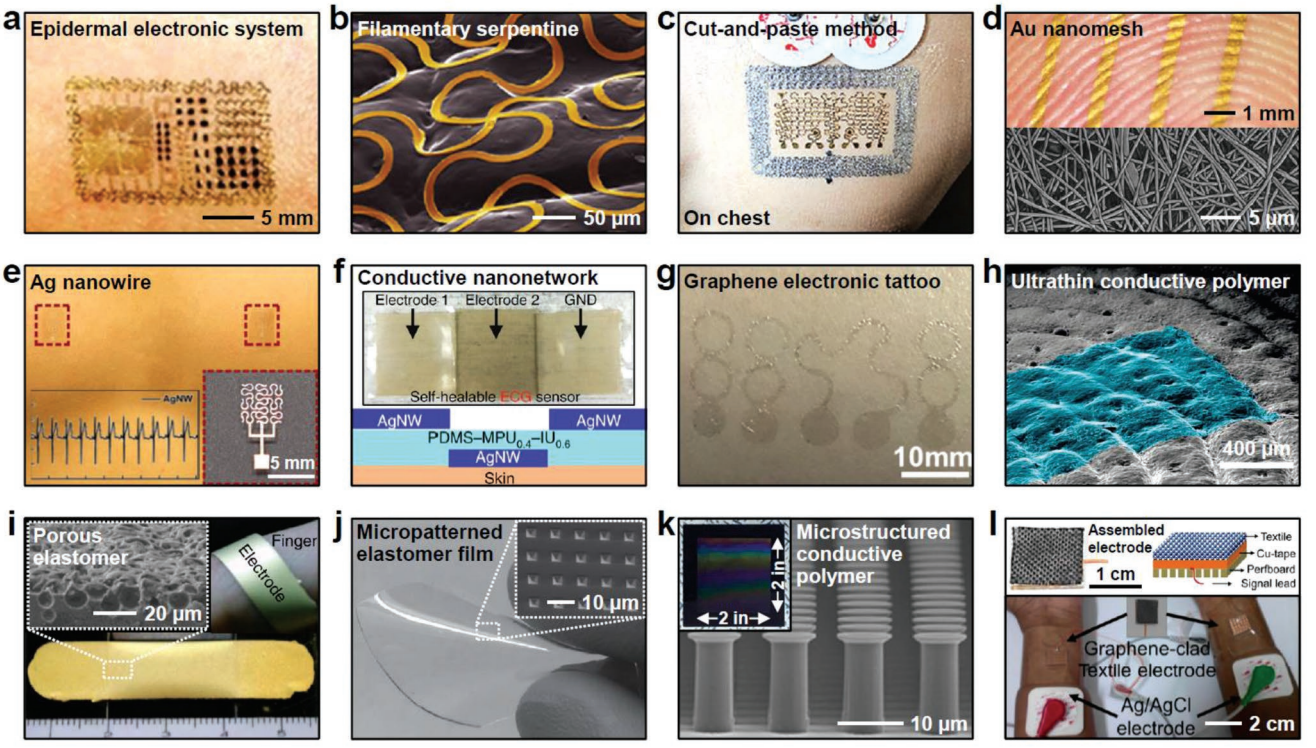

Figure 2. Skin-integrated electrode designs, materials, and structures of soft electronics for wearable ECG monitoring. a) Optical image of an epidermal electronic system on the skin integrating a metal-on-polymer FS design. Reproduced with permission.[37] Copyright 2011, AAAS. b) Colorized scanning electron microscopy (SEM) image of wearable soft electronics integrating a thin and narrow FS design strategy, which improves deformability. Reproduced with permission.[38] Copyright 2013, Wiley-VCH. c) Optical image of multiparametric epidermal sensor systems fabricated by a cost- and time-effective "cut-and-paste" method. Reproduced with permission.[43] Copyright 2015, Wiley-VCH. d) Optical image of substrate-free and ultrathin AuNM conductors on the skin (top) and an SEM image of the AuNM after dissolving the PVA nanofibers (bottom). Reproduced with permission.[51] Copyright 2017, Nature Publishing Group. e) Optical image of Ag NW-based dry ECG electrodes on the chest, the ECG signals collected by the electrodes on the chest (left inset), and a magnified optical image of an electrode fabricated by electrohydrodynamic printing (right inset). Reproduced with permission.[52] Copyright 2018, The Royal Society of Chemistry. f) Optical image of self-healable and stretchable AgNW electrodes (top) and a side view of the structure (bottom). Reproduced with permission.[53] Copyright 2017, Nature Publishing Group. g) Optical image of a sub-micrometer-thick transparent graphene electronic tattoo sensor. Reproduced with permission.[54] Copyright 2017, ACS Publications. h) Optical image of an unperceivable and ultrathin electrode with inkjet-printed PEDOT:PSS on the skin. Reproduced with permission.[55] Copyright 2018, Wiley-VCH. i) SEM image showing the side view of a porous PDMS film (top left), an optical image of a Au/Ti-deposited porous PDMS ECG electrode (bottom), and an optical image of the electrode wound around a finger (top right). Reproduced with permission.[56] Copyright 2013, Wiley-VCH. j) Optical image of a PGS biodegradable elastomer sensor. The inset shows an SEM image of square-pyramid-structured PGS film. Reproduced with permission.[57] Copyright 2013, Wiley-VCH. k) SEM image of gecko-inspired conductive micropillars with mushroom tips. The inset shows the large-area replicated conductive micropillars. Reproduced with permission.[58] Copyright 2016, ACS Publications. l) Optical image (top left) and a schematic (top right) of a graphene-clad textile electrode with reduced graphene oxide and nylon and the ECG measurement setup with the graphene-clad textile electrode (bottom). Reproduced with permission.[59] Copyright 2015, Elsevier.

also been demonstrated, showing higher patterning resolutions (up to 19 μm separation between lines).[48–50] In addition to Au thin films, Au nanomesh (NM) electrodes were invented to achieve thinness and stretchability simultaneously without any supporting substrate (Figure 2d). The porous AuNM electrodes also offer unprecedented breathability.[51]

Electrically conductive nanomaterials other than Au are also possible candidate materials for building surface electrodes. For example, Ag nanowire (AgNW)-based electrodes have been fabricated by electrohydrodynamic (EHD) printing, which allows the printing of conductive inks on a variety of unconventional substrates including paper and polymers (PET and polydimethylsiloxane (PDMS)) (Figure 2e).[52] Mixing AgNWs into a self-healable polymer matrix allowed the nanocomposite to recover its mechanical properties and electrical conductivity within seconds after damage. Therefore, self-healable surface electrodes could be achieved (Figure 2f).[53] As a semimetal, an atomically thin graphite layer called graphene is also a promising electrode material due to its biocompatibility, mechanical robustness, and chemical inertness. Since graphene is also mechanically cuttable, transparent graphene e-tattoos (GETs) have been successfully fabricated using the "cut-and-paste" method (Figure 2g).[54] In addition to inorganic nanomaterials, organic conductors such as poly(3,4-ethylene dioxythiophene):poly(styrene sulfonate) (PEDOT:PSS) can be inkjet-printed into nanomembranes as skin-conformable electrodes that show long-term stability (up to 48 h) (Figure 2h).[55]

Beyond planar electrodes, structurally engineered ECG electrodes can further enhance sensor performance or skin attachment. For example, Au and Ti electroplated porous electrodes are

flexible and directly solderable (Figure 2i).[56] The introduction of a microstructured dielectric layer of poly(glycerol sebacate) (PGS) between the electrode and the skin has enhanced the SNR and response time (Figure 2j).[57] Gecko-inspired conductive micropillars with mushroom tips can serve as both electrodes and dry adhesives that can repetitively attach to skin with good adhesion (Figure 2k).[58] Although the above mentioned electrodes are extra attachments, conductive fabrics have been fabricated as a natural interface with human skin. By dipping nylon fabric into a reduced graphene oxide (rGO) solution followed by a thermal treatment, graphene-based textile electrodes for ECG monitoring have been manufactured (Figure 2l).[59] However, without secure attachment to the skin, the ECG signals recorded by such textiles showed more baseline drift and motion artifacts compared to those recorded by conventional Ag/AgCl gel electrodes.

2.2. Soft Continuous ECG Sensors

Although the aforementioned soft electrodes are mainly driven by advancements in materials and fabrication processes, the creation of soft continuous ECG sensors has many more systematic challenges. Beyond soft electrodes, innovative structural designs for complete circuits, unconventional assembly strategies for integrated circuits (ICs), power supplies, and data transmission are demanded. Although the newly launched Apple Watch Series 4 has approval from US Food and Drug Administration (FDA) for ECG measurement, it requires two-handed operation, as an ECG has to be measured across the heart. Therefore, hands-free continuous ECG measurement require electrodes to be placed on the chest. Currently, there is an FDA-approved soft ECG monitoring device called Zio Patch (iRhythm Technologies Inc., USA) (**Figure 3**a).[60] It has dimensions of 123 mm × 53 mm × 10.7 mm.[61] Although the electrode areas are thin and flexible, the circuits, storage, and battery modules are lumped into a large rigid bump with a soft enclosure at the center of the patch. It can continuously record a single-lead ECG for up to 14 d, but it is not capable of streaming real-time ECG data. Instead, the ECG data are stored on board, which need to be downloaded after recording. Another commercial soft ECG sensor with FDA clearance is BioStamp nPoint (MC10 Inc., USA).[62,63] Its predecessor,

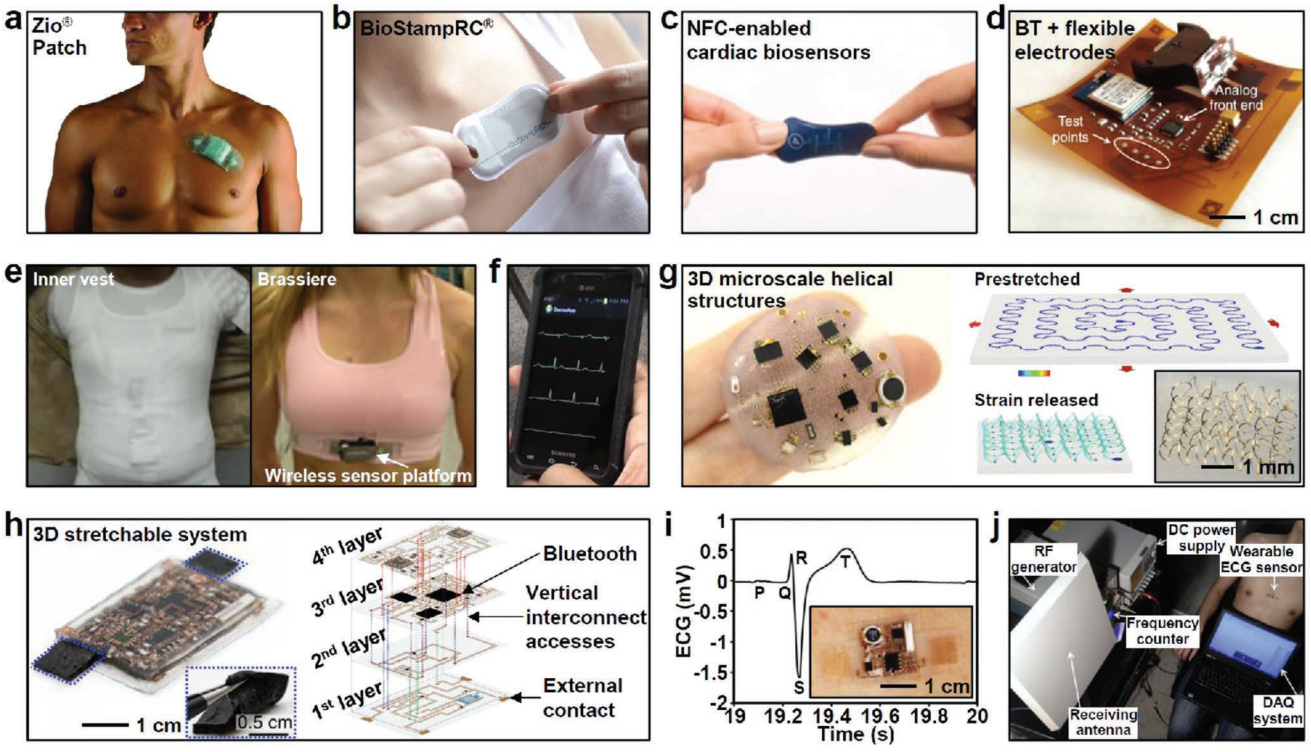

Figure 3. Soft continuous ECG sensors. a) Optical image of the single-lead Zio Patch (iRhythm Technologies Inc.) for recording ECG data for up to 14 d. Reproduced with permission.[60] Copyright 2014, Elsevier. b) Optical image of BioStampRC (MC10 Inc.), which captures surface biopotential signals. Reproduced with permission.[63] Copyright 2018, MC10 Inc. c) Optical image of NFC-enabled disposable cardiac biosensors integrated with batteries. Reproduced with permission.[35] Copyright 2018, Nature Publishing Group. d) Optical image of a double-sided inkjet-printed wearable ECG sensor patch integrated with a BT SoC. Reproduced with permission.[64] Copyright 2016, Wiley-VCH. e) Optical image of the textile-based ECG platforms for men (left) and women (right). Reproduced with permission.[66] Copyright 2014, The Electrochemical Society. f) Wirelessly transmitted real-time signals displayed on the smartphone. Reproduced with permission.[66] Copyright 2014, The Electrochemical Society. g) Optical image of the spiral network of 3D microscale helical structures for wireless soft electronics (left) and its finite element analyses (right). Reproduced with permission.[67] Copyright 2017, Nature Publishing Group. h) Optical image of 3D integrated stretchable electronics (left) and a schematic of multi-layer fabrication by a laser ablation method (right). Reproduced with permission.[71] Copyright 2018, Nature Publishing Group. i) ECG acquired with a microfluidic-chamber-enhanced stretchable ECG device by wireless data/power transfer. The inset shows an optical image of the microfluidic assemblies. Reproduced with permission.[72] Copyright 2014, AAAS. j) ECG measurement setup of the microfluidic assemblies in (i). Reproduced with permission.[72] Copyright 2014, AAAS.

BioStampRC, is a much thinner and even slightly stretchable single-lead ECG sensor that can wirelessly stream real-time ECG data to a mobile device via Bluetooth (BT) (Figure 3b). Stretchability is enabled by the island + bridge design. The integration of near-field communication (NFC) capability into the patch platform can activate the ECG sensor via an approaching cell phone (Figure 3c).[35] Although the overall patch is thin and slightly stretchable, BioStamp uses rigid dry electrodes.

Ultrathin Au electrodes can be flexible or even stretchable. Au electrodes have been inkjet-printed onto 50 μm thick Kapton sheets as flexible substrates (Figure 3d).[64] Kapton is a substrate material with a high thermal budget (400 °C), onto which ICs can be directly soldered to build a so-called BT system on a chip (SoC).[64] In addition, textiles were utilized as electrodes. Both inner vest (Figure 3e, left) and brassiere (Figure 3e, right) were incorporated with nanostructured dry textile electrodes and printed conductive ink traces with a sensor electronics module to capture surface biopotentials.[65,66] The electronics module is capable of wirelessly transmitting real-time ECG data via ZigBee (Figure 3f).

To build a truly skin-soft and stretchy wireless ECG sensor, the concept of a 3D architecture was used to replace in-plane serpentine structures. On an Ecoflex substrate, rigid ICs interconnected by a spiral network of 3D microscale helical structures demonstrated significant stretchability (>1.8 times) due to the uniformity in the stress distribution (Figure 3g).[67] Yamamoto et al. reported a multifunctional real-time cardiac monitoring patch with a modular design separating a reusable component and disposable components that address cost and hygiene concerns. The device is composed of three Ag electrodes printed onto a 38 μm thick PET film.[68,69] However, the device must be wired with an external power source and a data link for data processing since signal processing components, amplifiers, and filters are not integrated into the device itself. The PET substrate cannot induce a sufficient conformability with skin; thus, additional conductive medical grease was applied to enhance the contact between the electrodes and the skin. Liu et al. demonstrated a soft, conformal class for a wired mechano-acoustic-electrophysiological sensing platform. The collection of ECG and mechano-acoustic signals such as a seismocardiogram (SCG) on the chest is enabled by integrating capacitive electrodes, a digital accelerometer, and active filter components into the device.[70]

To increase functionalities, the area limitation of a single-layer circuit becomes a major issue. To resolve such a limitation, the 3D stacking of soft circuits has been proposed. By laser manufacturing, a 3D stretchable circuit employed a soft elastomer as the dielectric layer between layers (Figure 3h).[71] Vertical interconnect accesses can be fabricated through the laser ablation of the elastomer layers. With an external battery, a stretchable patch with 3D stacking is able to transmit a real-time ECG and motion via BT.

Long-term power still remains a significant challenge for wearable devices. Therefore, multiple wireless powering/charging strategies have been implemented. For example, radio-frequency (RF) data/power transmission has been implemented in a microfluidic-chamber-enhanced stretchable ECG device (Figure 3i).[72] However, to allow for fully wireless data/power transmission, a combination of relatively bulky external waveform generators, receiving antennas, frequency counters, and/or power supply modules are necessary (Figure 3j).[72]

2.3. Wearable Pulse Oximeters

While a continuous ECG has to be measured from the chest, continuous measurement of the blood oxygen saturation (SaO_2) can be carried out at the fingertip or wrist using flexible pulse oximeters (Figure 1a, right).[73] In the blood,[74] O_2 is dissolved and selectively binds to hemoglobin, forming a mixture of oxyhemoglobin (binding and transporting oxygen, HbO_2) and deoxyhemoglobin (without bound oxygen, Hb) in the blood. The percent saturation of HbO_2 in arterial blood is the SaO_2.[75] When measured by a pulse oximeter, it is termed the SpO_2. A conventional rigid pulse oximeter clips onto a fingertip. It consists of a photodetector (PD) and two quickly alternating light-emitting diodes (LEDs) with differing wavelengths such as IR (940 nm) + red (660 nm) or green (530 nm) + red. Depending on the application, the PD and LEDs are placed vertically,[75,76] as in the transmission mode (**Figure 4**a), or horizontally,[77–80] as in reflection mode. Figure 4b illustrates the transmitted light pathway of upward incident light to the PD.[73] The light has to transfer through arterial blood, venous blood, and other tissue. The light absorption consists of a pulsating alternating-current (AC) signal caused by the systole (maximum light absorption) and diastole (minimum light absorption) in the artery, and a nonpulsating direct-current (DC) signal from the venous blood and tissue. To calculate the SpO_2, the incident light of the DC- and AC-component signals from the LEDs are used in accordance with the Beer–Lambert law because HbO_2 and Hb have different absorption rates at different wavelengths.[81] The SpO_2 of healthy people ranges from 95 to 99%. In combination with the pulse, the SpO_2 is an expeditious way to detect abnormal cardiovascular activity.[73]

Bulky and rigid commercial pulse oximeters are obstructive to wear and therefore inapplicable for continuous SpO_2 sensing. As a result, more "skin-like", flexible and stretchable[82,83] pulse oximeters demonstrate conformability to the skin with thin and lightweight form factors, as well as integration of soft materials for mechanical robustness and elastic deformations. Flexible organic LEDs (OLEDs) and organic PDs (OPDs) have become good candidate active materials for flexible oximeters.[73,77,78,84] Lochner et al. used polyfluorene derivatives as the emissive layers of OLEDs, and the active layer of OPDs were printed on a planarized polyethylene naphthalate (PEN) substrate using a blade-coating technique. Red and green OLEDs were fabricated with peak wavelengths at 626 and 532 nm, respectively. Comparable to the conventional combination of red and near-IR LEDs, the red and green OLEDs are able to calculate the SpO_2. The OLEDs and OPDs are arranged in the transmission mode, but their rigidity limits the flexibility of such oximeters (Figure 4c).[73] Reflection-mode pulse oximeters were demonstrated with red and green OLEDs and a Si PD placed on the same side (Figure 4d).[78] As such an arrangement requires more space on one side, the wrist is a more practical location.

NFC-enabled wireless pulse oximeters as a finger wrap (Figure 4e)[77] or nail patch (Figure 4f)[79] have also been reported. The ultraminiaturized (10 mm in diameter, 0.9 mm

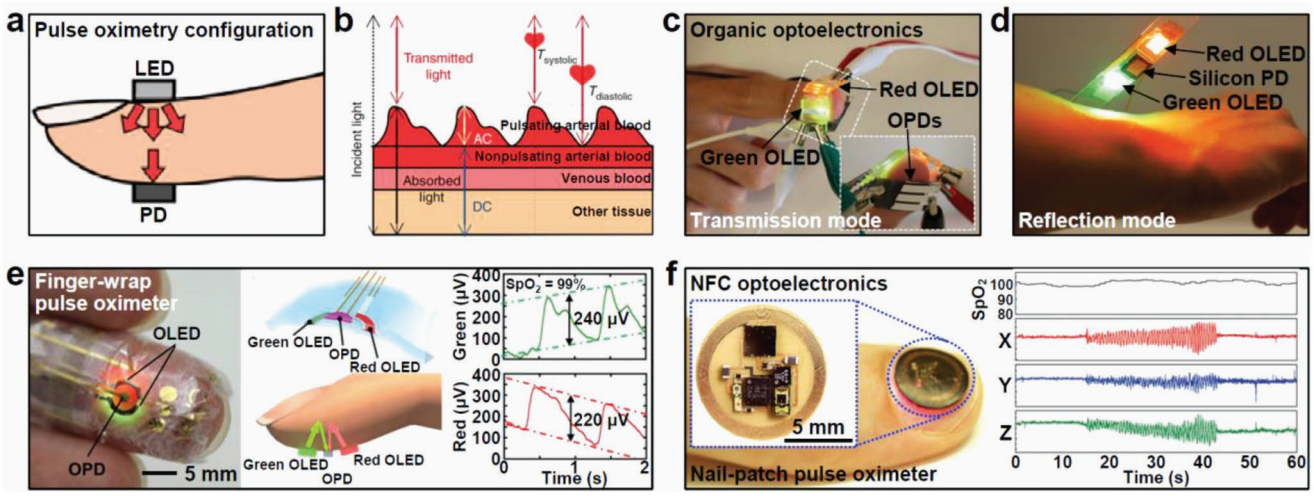

Figure 4. Wearable pulse oximeters. a) Principle of pulse oximetry operation. The light emitted from an LED is collected by a PD. Reproduced with permission.[76] Copyright 2014, MDPI. b) Pathway of the transmitted light of the incident light with pulsating and nonpulsating transmission signals. Reproduced with permission.[73] Copyright 2014, Nature Publishing Group. c) Optical image of transmission-mode pulse oximetry composed of red and green OLEDs and printed OPDs. The inset shows an optical image of the bottom view of pulse oximetry. Reproduced with permission.[73] Copyright 2014, Nature Publishing Group. d) Optical image of reflection-mode pulse oximetry using flexible blade-coated red and green OLEDs and a Si PD. Reproduced with permission.[78] Copyright 2017, Wiley-VCH. e) Thin and flexible red and green OLEDs and an OPD wrapped on a finger (left), the structure of the devices (top center), operation principle of reflection-mode pulse oximetry (bottom center), and the OPD signal output from the incident green and red OLEDs for 99% oxygenation of the blood (right). Reproduced with permission.[77] Copyright 2016, AAAS. f) Optical image (left) and magnified image (left inset) of an NFC-enabled nail-patch pulse oximetry system. The SpO_2 was extracted from the nail-patch pulse oximeter, and movement artifacts were measured with an accelerometer affixed to the finger (right). Reproduced with permission.[79] Copyright 2016, Wiley-VCH.

in thickness) and lightweight nail patch is securely attached to a nail through a biocompatible adhesive. The adhesive is crucial for the minimization of motion artifacts, as evident in the right panel of Figure 4f.[79]

2.4. Invasive Soft Cardiac Monitoring Sensors

In addition to ECG, BP is also an important indicator to monitor cardiovascular health. The ECG measures electrical activity of the heart, which is analyzed by measuring the time intervals, magnitudes, and shapes of the waveform. This gives insight into the regularity of a heartbeat, how long a signal takes to pass through the chambers, size of the heart, etc. Unlike ECG, BP is closely related to hemodynamics of the cardiovascular system. Hence, BP values in various chambers of the heart (left/right side of the heart) and in the vascular system (central/peripheral) aid the physician to determine the functional integrity of the cardiovascular system that is affected by cardiac power, arterial stiffness, blood flow resistance, and blood viscosity.[85] The pressures generated by the left (arterial pressure) and right side (venous pressure) of the heart differ in pulse wave shape and peak values. It is imperative to consider these differences and to monitor minute changes continuously.[85–87]

Although soft wearable cardiovascular sensors are becoming more capable and long-term, many localized and accurate electrophysiological signals still require in vivo measurement directly from the heart surface (Figure 1b, right)[88–90] or the blood vessels (Figure 1b, left).[91–96]

A continuous BP-sensing arterial line (a-line) is a good example. Noninvasive inflatable BP cuffs on the arm or wrist (sphygmomanometry) are very bulky to wear and can only offer discrete measurements. There are several other noninvasive BP estimation techniques such as volume clamping,[97] arterial tonometry,[98,99] ultrasound wall-tracking, and pulse transit time (PTT). Recently, an ultrasonic device featuring a wearable form factor (thickness: 240 μm) and skin conformability was reported with resolution that is comparable to medical ultrasonic probes.[87] However, none of these methods have FDA approval for continuous BP measurement owing to their limited accuracy and wearability. Therefore, the currently invasive a-line is the only gold standard for continuous BP sensing. Making wirelessly operating a-line can enable a fully implantable and continuous BP sensor. Cleven et al. reported such a wireless and battery-free system composed of a complementary metal–oxide–semiconductor (CMOS) chipset (5.6 mm × 0.7 mm × 350 μm) with an integrated application-specific integrated circuit (ASIC), which can measure the BP with a sampling rate of 30 Hz and has a measurement range of 30–300 mmHg (blood-pressure in the femoral artery of a sheep) and an accuracy of ±1.0 mmHg (**Figure 5**a).[95] The sensor is powered via inductive coupling with an external reader station and must be implanted into the femoral artery in order to gain access to the vessel using the Seldinger technique. Although this procedure is less invasive than standard cardiac catheter examination, the insertion of this device requires puncturing the desired vessel, which would increase the risk for the patient compared to standard a-line procedures.

Monitoring peripheral BP (brachial, wrist, fingers) has become widespread, but it is important to consider that BP (both systolic and diastolic) varies depending on its measurement location and position throughout the arterial tree.[100]

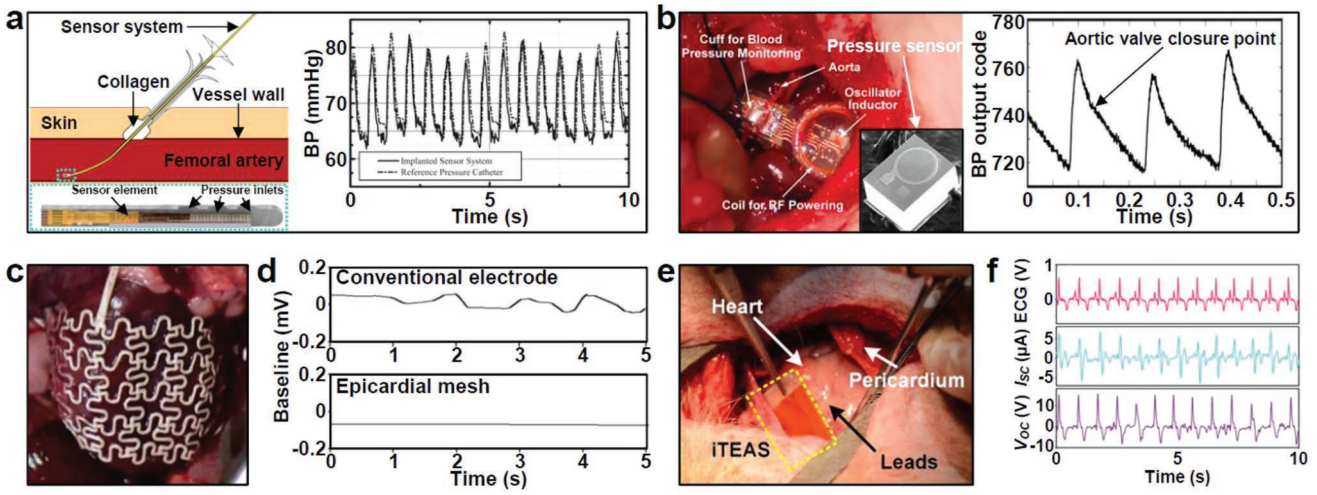

Figure 5. Invasive soft cardiac monitoring sensors. a) Procedure for implanting the wireless CMOS chipset system integrated with a membrane capacitive pressure sensor and an ASIC (left) and the wirelessly transmitted measured BP from a sheep under anesthesia (right). Reproduced with permission.[95] Copyright 2012. IEEE. b) Optical image of an implantable silicone cuff-based BP sensing microsystem wrapped around a blood vessel (left). The inset shows an SEM image of the capacitive pressure sensor. The BP waveform for a laboratory mouse was wirelessly measured with the device (right). Reproduced with permission.[91] Copyright 2009. IEEE. c) Optical image of an elastoconductive mesh electrode composed of a nanocomposite of AgNWs and SBS. Reproduced with permission.[90] Copyright 2016, AAAS. d) ECG baseline drift of the conventional and epicardial meshes in c). Reproduced with permission.[90] Copyright 2016, AAAS. e) Optical image of a self-powered iTEAS implanted near a pig heart. Reproduced with permission.[89] Copyright 2016, ACS Publications. f) In vivo output performance for the implanted iTEAS in e). Reproduced with permission.[104] Copyright 2016, ACS Publications.

Although peripheral BP is accepted as an important predictor for certain symptoms, recent studies have shown the importance of central BP.[101] Assessment of central BP rather than peripheral BP may improve the identification of cardiovascular health, as shown in a BP lowering drug test.[102,103] From that perspective, Cong et al. demonstrated real-time BP measured from aorta. To avoid puncturing a blood vessel, a pressure-sensing silicone cuff wrapped around the blood vessel has been instrumented (Figure 5b).[91] The elastic cuff is composed of a micro-electromechanical systems (MEMS) capacitive pressure sensor (Figure 5b, inset), which is immersed in a low-viscosity silicone oil. The BP waveform is measured by coupling the cavity modulation caused by a change in the vessel volume, and a strain gauge measuring the change in the diameter with a linear sensitivity of 0.18% $mmHg^{-1}$ of the base capacitance (in vivo). Unlike the conventional catheter-based approach, this device circumvents complications such as vessel occlusion, bleeding, and blood clotting.

Soft electronics are not only able to wrap around blood vessels but also the beating heart to measure intrinsic myocardial electrical activities. Such devices should have mechanical properties to enable wrapping of the heart with a reasonable contact pressure for attachment and conformability but with minimal mechanical resistance to the natural heartbeat. An elastoconductive mesh electrode composed of a homogeneous nanocomposite of AgNW and biocompatible styrene–butadiene–styrene (SBS) rubber was demonstrated to resemble the elastic and electrical characteristics of cardiac tissue (Figure 5c).[90] This cardiac mesh has been successfully integrated into the epicardial surface and monitored the surface ECG with less baseline drift than conventional bipolar electrodes (Figure 5d).[90]

The operation of implantable electronic devices is significantly constrained by the power supply. Even if they are wirelessly powered by an external RF source, an RF generator has to be held nearby, which still limits mobility. Ideally, the implantable device can be self-powered by harvesting mechanical energy from the heart.[89,104] An implantable triboelectric active sensor (iTEAS) (Figure 5e) was demonstrated to be able to self-generate an open-circuit voltage (V_{OC}) of 10 V and a short-circuit current (I_{SC}) of 4 μA (Figure 5f).[89] Without a battery, it was able to continuously monitor multiple cardiac signals such as heart rates, respiratory rates, ECGs, and the estimated BP.

Continuous measurement of blood flow also plays an important role in the diagnosis and characterization of cardiovascular health by providing microvascular and macrovascular flow information regarding kinetic energy along its course through the body. Abnormal blood flow patterns caused by abnormal geometry of vessels or valves induce unavoidable frictional loss of energy, hence it may ultimately result in heart failure.[105] There are several principles to measure blood flow including mechanical, optical, acoustic, and thermal methods. Webb et al. reported an epidermal device that allows for precision thermal measurements of blood flow. This flexible and thin device can monitor both the speed and direction of surface (up to 2 mm in depth) blood flow quantitatively.[106]

2.5. Soft Epicardial Mapping Devices

Invasive epicardial sensors are also capable of cardiac mapping with a high spatiotemporal resolution. Real-time mapping and the modulaton of the electrophysiology of in vivo cardiomyocytes could have significant impacts on the cardiac activity

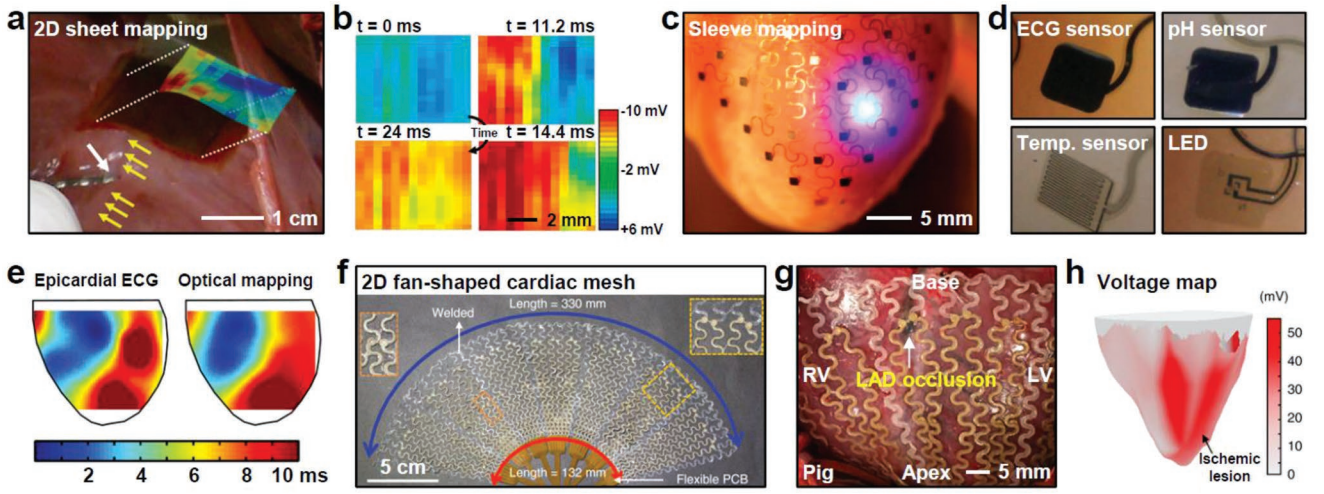

Figure 6. Soft epicardial mapping devices. a) Optical image of a flexible electronic sensor system conforming to a pig heart with overlaid mapping results of the relative depolarization response. Left anterior descending (LAD) coronary artery (yellow arrows) and the pacing electrode (white arrow). Reproduced with permission.[107] Copyright 2016, AAAS. b) Cardiac activation voltage maps at four different time points. Reproduced with permission.[107] Copyright 2016, AAAS. c) Optical image of 3D-MIMs laminated on a rabbit heart. Reproduced with permission.[110] Copyright 2014, Nature Publishing Group. d) Magnified images of the electrical (top left), pH (top right), and temperature (bottom left) sensing elements and an LED (bottom right) integrated in (c). Reproduced with permission.[110] Copyright 2014, Nature Publishing Group. e) Spatial activation maps measured by the 3D-MIMs in (c) (left) and a conventional optical mapping (right). Reproduced with permission.[110] Copyright 2014, Nature Publishing Group. f) Optical image of a 2D fan-shaped cardiac mesh composed of Au-coated AgNWs in SBS elastomer. Reproduced with permission.[111] Copyright 2018, Nature Publishing Group. g) Optical image of the cardiac mesh in (f) implanted on a pig heart. Reproduced with permission.[111] Copyright 2018, Nature Publishing Group. h) Voltage map constructed from the intracardiac recording by the cardiac mesh in (f). Reproduced with permission.[111] Copyright 2018, Nature Publishing Group.

in clinical therapy (Figure 1b, right).[96] Soft cardiac mapping devices in various forms such as 2D sheets,[107–109] sleeves,[110] and meshes[90,111] have been demonstrated for recording and stimulating a multitude of sites on the heart (**Figure 6**). These devices are required to be fully isolated from biological fluids in order to prevent current leakage that can cause unintended shock in adjacent tissues. An electronic sensor system conforming to the epicardium via surface tension and composed of 288 multiplexed Si nanomembrane channels was configured to measure cardiac activity (Figure 6a).[107] The relative activation time at each contact point was used to visualize the propagation of cardiac depolarization (Figure 6b). The 48 μm thick circuits allowed the system to be rolled up and delivered via catheter.[107]

Such flexible active arrays of 2D sheet-like mapping devices have limitations such as the coverage area and the reliability of the contact with the epicardial surface. Therefore, 3D multifunctional integumentary membranes (3D-MIMs) represent a major breakthrough in soft epicardial electronics because they are the first to achieve spatiotemporal mapping across the entire epicardium of both the anterior and posterior surfaces (Figure 6c).[110] High-density electrical, pH, and temperature sensors and LEDs integrated into 3D-MIMS are capable of ECG, pH, and temperature mapping and optical stimulation (Figure 6d). In vivo experiments on rabbit hearts validated the spatiotemporal mapping capability of 3D-MIMS against the conventional optical measurement of voltage-dependent fluorescence (Figure 6e).[110]

However, it is challenging to extend the validity of these devices in human cardiac models based on in vivo experiments on small animal models because of the innate physiological discrepancies between small and large animals. Hence, large-animal models need to be used. Recently, a large-area conductive nanocomposite mesh was applied to a pig heart for in vivo measurements (Figure 6f).[111] The cardiac mesh is composed of Au-coated AgNWs in an SBS elastomer configured in a 2D mesh with a fan shape with 42 electrodes integrated throughout it. This mesh was designed to cover the entire ventricle surface of a pig heart with a high conductivity (41 850 S cm^{-1}) and stretchability (266%) (Figure 6g). An in vivo voltage map of the anterior and posterior of the heart can be obtained using this mesh (Figure 6h).[111]

3. Soft Bioelectronics–Assisted Therapy

3.1. Soft Bioelectronics–Integrated Pacing and Defibrillation

A heartbeat originates from the SA node—the endogenous pacemaker.[112] The electrical impulse produced by the SA node initiates the contraction of the left and right atria and travels down to the atrioventricular (AV) node. The electrical impulse travels further down to the His bundle and then the Purkinje fibers, which triggers the contraction of the ventricles. When this CCS is not functioning properly, the heart rate and rhythm of the heartbeat may be abnormal (a condition called arrhythmia). There are many causes (e.g., smoking, diabetes, hypertension, alcohol, and stress) and types (tachycardia, bradycardia, atrial fibrillation, and ventricular fibrillation) of arrhythmia. Failure of the SA node to generate an electrical impulse or block during the propagation of an electrical impulse to the ventricles can slow the heartbeat (a condition called bradycardia). Pacemakers, which consist of a pulse

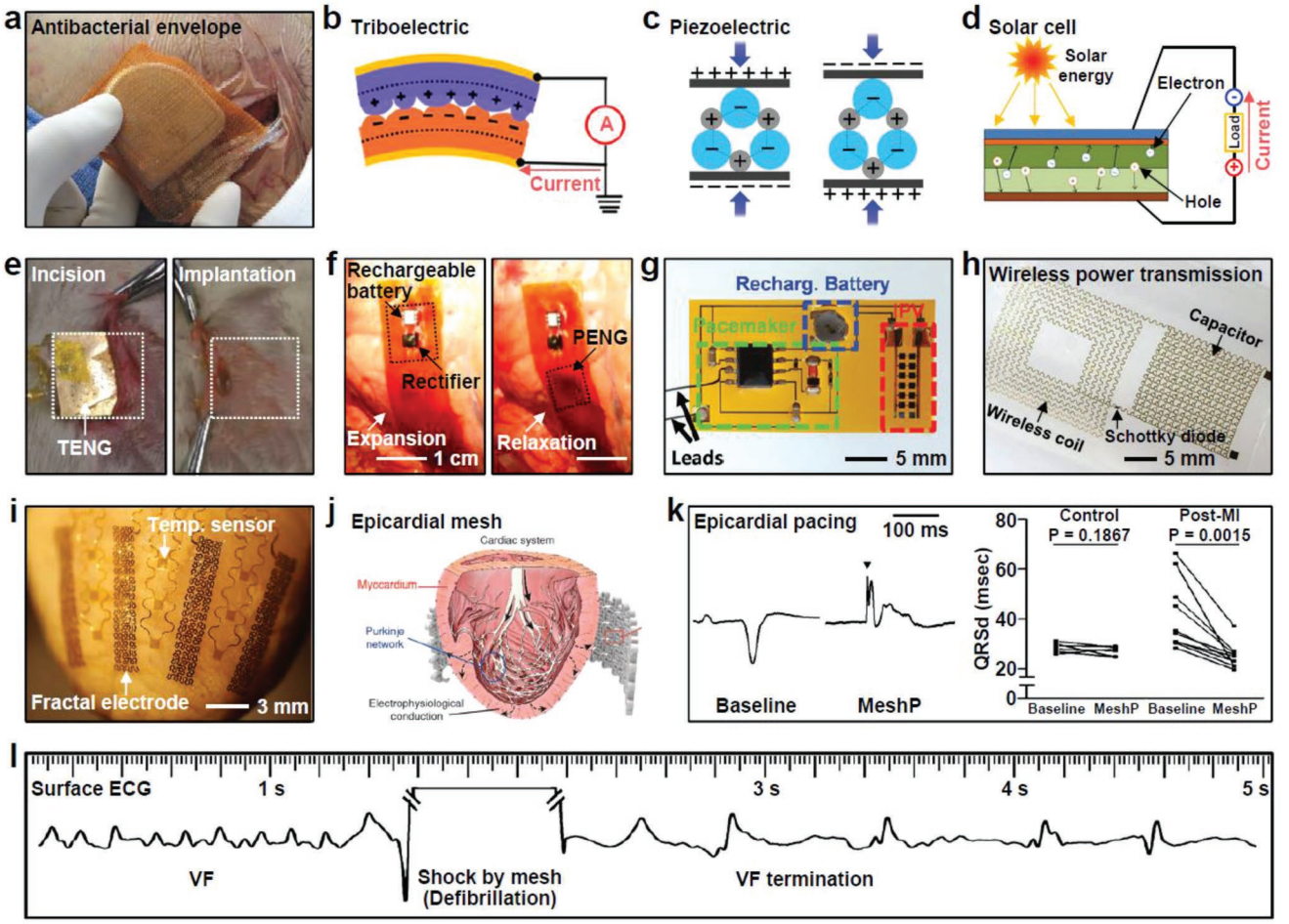

Figure 7. Soft bioelectronics–integrated pacing and defibrillation. a) Optical image of an antibacterial envelope (TYRX, Medtronic Inc.) for an implantable pacemaker. Reproduced with permission.[120] Copyright 2011, Springer Healthcare. b) Schematic of the energy harvesting mechanism of a TENG. Reproduced with permission.[157] Copyright 2012, Elsevier. c) Schematic of the energy harvesting mechanism of a PENG. Reproduced with permission.[153] Copyright 2016, Wiley-VCH. d) Schematic of the energy harvesting mechanism of a solar cell. Reproduced with permission.[158] Copyright 2014, Hindawi Publishing Corporation. e) Optical images of before (left) and after (right) implanting a TENG (white dotted box) under rat skin. Reproduced with permission.[131] Copyright 2014, Wiley-VCH. f) Optical images of a flexible energy harvester with a PENG, a rechargeable battery, and a rectifier mounted on a bovine heart during the expansion (left) and relaxation (right) phases. Reproduced with permission.[137] Copyright 2014, National Academy of Sciences. g) Optical image of a solar-powered flexible pacemaker with a rechargeable battery. Reproduced with permission.[143] Copyright 2016, Wiley-VCH. h) Optical image of a stretchable wireless charging system. Reproduced with permission.[148] Copyright 2013, Nature Publishing Group. i) Optical image of a 3D-MIM with fractal electrodes laminated on a rabbit epicardial surface. Reproduced with permission.[160] Copyright 2015, Wiley-VCH. j) Schematic of an epicardial mesh composed of AgNWs and SBS rubber wrapped around the epicardium. Reproduced with permission.[90] Copyright 2016, AAAS. k) ECGs before and after pacing with the epicardial mesh in (j) (left) and the QRS durations in control and postmyocardial infarct rats (right). Reproduced with permission.[90] Copyright 2016, AAAS. l) ECG monitored during ventricular fibrillation (VF), defibrillation, and VF termination. Reproduced with permission.[90] Copyright 2016, AAAS.

generator and leads, are implanted on the patient's chest to treat bradycardia (Figure 1c, top right).[113] They monitor the heartbeat of the patient and send an electrical impulse when the heartbeat is too slow.

One of the major limitations of a pacemaker is pocket infection caused by the implanted device and the limited battery lifespan of the pulse generator.[114–119] Serious infections can lead to lethal complications such as urosepsis, wound dehiscence, and erosion at the pocket site. An FDA-approved antibacterial envelope—a poly(propylene) mesh that releases antimicrobial agents including rifampin and minocycline (TYRX, Medtronic Inc., USA)—has shown significant efficacy in reducing the risk of infection (**Figure 7**a).[120–129]

Another major limitation of a pacemaker is the limited lifespan of the battery, and this necessitates additional surgical procedures to replace the discharged battery.[130] Soft bioelectronic devices that can generate power, including triboelectric (Figure 7b),[131–136] piezoelectric (Figure 7c),[137–142] solar-powered (Figure 7d),[143–147] and wirelessly powered devices,[130,148–151] are especially promising for overcoming the limited battery life because they are thin, lightweight, and biocompatible, ideal for implantable device applications.[152–157]

Flexible triboelectric nanogenerators (TENGs) convert mechanical energy into electrical energy by utilizing triboelectrification and electrostatic induction (Figure 7b).[157] A TENG operates in the contact/separation cycles of two polymeric films with different electron-attracting abilities. Since the body possesses periodic and spontaneous mechanical motions such as breathing and heartbeat, implanted flexible TENGs can harvest energy from the body. For the in vivo application of a TENG, careful encapsulation with a biocompatible soft material is required because body fluids can deteriorate the performance of the TENG. Results from an in vivo application demonstrated on a living rat showed that a flexible TENG comprising PDMS micropatterned with a pyramid array, a PI substrate deposited with Au, an Al foil, and PET spacers could generate V_{OC} = 3.73 V and I_{SC} = 0.14 μA from rat breathing (Figure 7e).[131] The energy generated with five breaths could stimulate a single pulse comparable to a commercial pacemaker. Since the implanted TENG was designed to fit into the rat, a TENG for human application could be larger and would generate sufficient energy for stimulation with each breath.

Flexible piezoelectric nanogenerators (PENGs) utilize piezoelectric materials such as ZnO, lead zirconate titanate (PZT), $BaTiO_3$, and polyvinylidene fluoride to convert mechanical energy into electrical energy (Figure 7c).[152–154] A piezoelectric potential is generated when the central symmetry in the crystal structure of the piezoelectric material is broken by any type of external force. Similar to TENGs, PENGs operate in the bending/unbending cycles of piezoelectric materials, and an AC is generated. A flexible PZT-based PENG integrated with a rechargeable battery and rectifier could successfully harvest energy from the heart, lungs, and diaphragm of bovines and sheep (Figure 7f).[137] Since a single layer of a PZT-based PENG produced an insufficient amount of energy (3.7 V, 0.18 μW cm^{-2}) to operate a pacemaker (0.3 μW), five layers of PENGs were stacked, and the generated voltage and power density were 8.1 V and 1.2 μW cm^{-2}, which are sufficient to operate a cardiac pacemaker.

Flexible solar cells convert solar energy into electrical energy by a photovoltaic effect in which light absorption generates electron–hole pairs (Figure 7d).[158] Since sunlight can penetrate skin, a subdermal flexible solar cell would power a cardiac pacemaker. Fourteen dual-junction solar microcells (GaInP/GaAs) were integrated with a custom-built flexible pacemaker and rechargeable battery (Figure 7g).[143] This system was then implanted under the skin of a live hairless mouse. The values of V_{OC} and I_{SC} generated by the solar microcells were 4.6 V and ≈195 μA, which are sufficient to operate the custom-built flexible pacemaker (1.5–2 V, 76–105 μA). In addition, a stretchable and rechargeable battery integrated with a stretchable wireless power transmission system would be another alternative power source (Figure 7h).[148] The power is transferred by the inductive coupling of coils inside and outside the body, and a Schottky diode serves as a rectifier, which converts an AC into a DC.

Ventricular fibrillation, another type of arrhythmia, is the state in which disorganized electrical activity in the ventricles fails to squeeze blood from the ventricles. Strong electrical shocks, known as defibrillation, are applied to the ventricles to organize electrical activity and treat ventricular fibrillation.[159] To effectively deliver an electrical shock to the ventricles, fractal electrodes on a 3D-MIM that conform to the epicardium were fabricated (Figure 7i).[160] In a more recent report, an epicardial mesh comprising AgNW and SBS rubber was wrapped around the epicardium of postmyocardial infarction (post-MI) rats for mechanical support, biventricular pacing, and defibrillation (Figures 5c and 7j).[90] To evaluate the effect of biventricular pacing, electrograms before and after epicardial mesh pacing were measured (Figure 7k, left). With epicardial mesh pacing, the QRS durations, i.e., the total activation times of the ventricles, for post-MI rats were normalized (Figure 7k, right). When ventricular fibrillation spontaneously occurred for post-MI rats, a biphasic electrical shock with an energy of 2 J was delivered by an epicardial mesh, successfully terminating ventricular fibrillation (Figure 7l).

3.2. Soft Robotic Sleeves

Heart failure is a life-threatening chronic condition in which the heart muscle fails to circulate blood. Treatment options for end-stage heart failure include heart transplantation and left ventricular assist devices (LVADs).[161–166] In terms of long-term survival and quality of life, heart transplantation is thought to be the best option. However, the relative contraindications for the elderly (age limit of 70 years old) and long waitlist due to the limited donor pool necessitate other treatment methods as destination therapy or bridge-to-transplantation therapy (BTT).[167,168]

LVADs were initially designed as a BTT and later received attention as a destination therapy (**Figure 8**a).[161,169,170] An implanted pump, part of an LVAD, withdraws blood from the left ventricle (LV) and returns the blood back to the aorta. Consequently, a parallel path for blood flow is formed, which alleviates the pressure and volume applied to the LV. This mechanical unloading substantially improves the ventricular function and leads to a process called reverse remodeling.[171–174] However, since the blood directly contacts the LVAD, the LVAD is vulnerable to driveline infection, thromboembolism, and hemolysis. Therefore, patients are subjected to a lifetime of anticoagulant medication to prevent the clotting of blood.[175,176]

Meanwhile, passive ventricular restraint devices such as CorCap (Acorn Cardiovascular Inc., USA)[177,178] and HeartNet (Paracor Medical Inc., USA)[179–181] are not in contact with blood and wrap ventricles to reduce the ventricular wall stress and to limit the size of the dilated heart (Figure 8b–d). CorCap is an inelastic polyester mesh wrap that is sutured to the epicardium after median sternotomy, limiting the end-diastolic volume (Figure 8b).[177] HeartNet comprises a nitinol mesh and is more appealing than CorCap in that it is delivered by minimal incision left thoracotomy, and its elastic properties enable continuous compression against the epicardium (Figure 8c).[179] However, both of them failed to benefit long-term survival, and the level of restraint was not adjustable once deployed. To measure and optimize the level of restraint, a fluid-filled pressure-adjustable balloon was developed (Figure 8d).[182–184] A restraint level of ≈3.63 mmHg resulted in ≈10% reduction in cardiac output, which is sufficient to restrain eccentric hypertrophy after MI.

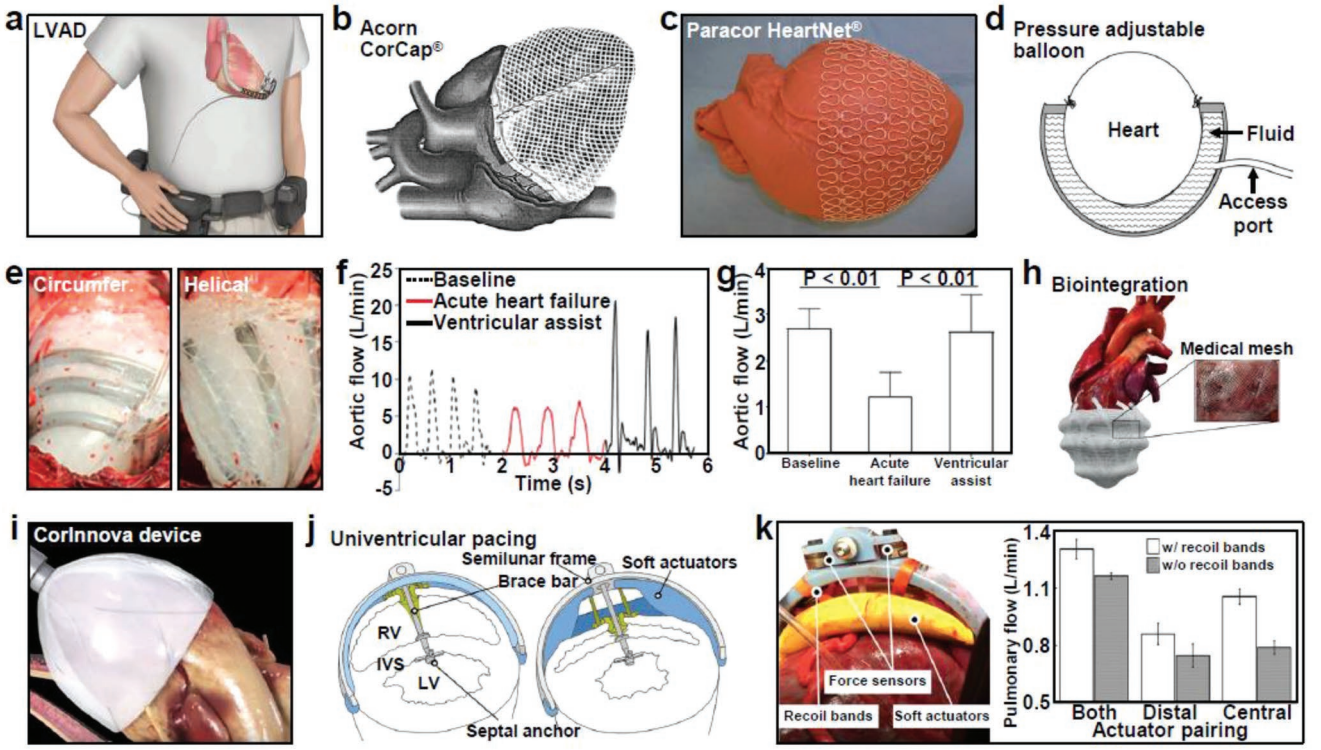

Figure 8. Soft robotic sleeves. a) Schematic of an LVAD. Reproduced with permission.[170] Copyright 2017, BMJ Publishing Group. b) Schematic of CorCap (Acorn Cardiovascular Inc.), an inelastic polyester mesh wrap, wrapped around the heart. Produced with permission.[177] Copyright 2002, Elsevier. c) Optical image of HeartNet (Paracor Medical Inc.), a passive ventricular restraint device made of a nitinol mesh, wrapped around a heart model. Reproduced with permission.[179] Copyright 2008, Elsevier. d) Schematic of a fluid-filled pressure-adjustable balloon ventricular restraint device. Reproduced with permission.[182] Copyright 2010, Elsevier. e) Optical image of McKibben soft actuators circumferentially (left) and helically (right) oriented. Reproduced with permission.[187] Copyright 2017, AAAS. f) Aortic blood flow rate of a pig heart before (black dotted line) and after inducing heart failure (red line), and with the assistance of the sleeve in e) (black line). Reproduced with permission.[187] Copyright 2017, AAAS. g) Average aortic blood flow rate for 10 consecutive cycles in six animals for the conditions in (f). Reproduced with permission.[187] Copyright 2017, AAAS. h) Optical image of soft-robotic-sleeve biointegration using medical mesh. Reproduced with permission.[193] Copyright 2018, Springer Nature. i) Schematic of CorInnova device (CorInnova Inc.) on the heart. Reproduced with permission. Copyright 2017, CorInnova. j) Schematic of a univentricular-pacing soft robotic device, composed of a semilunar frame, soft actuators, a brace bar, and a septal anchor, placed on the right ventricle (RV) during the diastolic (left) and systolic phases (right) (LV: left ventricle; IVS: interventricular septum). Reproduced with permission.[198] Copyright 2017, AAAS. k) Optical image of the in vivo measurement setup of the soft robotic device in (j) integrated with force sensors and recoil bands (left) and the pulmonary flow rates with (w/) and without (w/o) recoil bands (right). Different actuator pairings were activated (distal and/or central pairs). Reproduced with permission.[198] Copyright 2017, AAAS.

Recently, the integration of soft robotics pioneered a new field of more active and multifunctional treatment devices called soft robotic sleeves (Figure 1c, bottom right).[185,186] A soft robotic sleeve is wrapped around both ventricles to augment heart function.[187,188] A soft robotic sleeve consists of two layers of soft actuators stacked together that can act independently from each other. Inspired by actual hearts which consist of two layers of heart muscle that undergo twisting or compressive motions,[189] soft pneumatic artificial muscles called McKibben actuators are helically and circumferentially oriented (Figure 8e).[187] The soft actuator mimicking native heart muscle can elongate and contract and is made of silicone-based materials whose stiffness is similar to that of heart muscle.[190,191] The ECG, flow rate, and pressure were monitored to synchronize the soft robotic sleeve with the native cardiac cycle.[192] The effectiveness of soft robotic sleeves was demonstrated in vivo for acute heart failure induced in pigs. The aortic blood flow rate was monitored before (baseline) and after inducing heart failure, and with the assistance of a sleeve (Figure 8f). The average cardiac output decreased to ≈45% of the baseline after inducing acute heart failure but recovered to ≈97% of the baseline with the assistance of a sleeve (Figure 8g).

For efficient assistance by a sleeve, coupling of the sleeve to the epicardium is important, and various coupling methods were deployed, including sutures, suction, and surgical adhesives. Recently, a new concept of biointegration has been suggested to couple a sleeve to the epicardium, in which cell migration into interface materials enhances adhesion.[193] In this strategy, a soft robotic sleeve using medical mesh as an interface material was fabricated, implanted on the heart, left over for tissue integration into the medical mesh, and then actuated for cardiac assistance (Figure 8h). The medical mesh implanted for 14 d endured a pull-off force of 2.27 N, as compared to 0.91 N for a silicon implant. The first soft robotic device (CorInnova Inc., USA) that can be delivered by a minimally invasive method through

a delivery tube was designed (Figure 8i).[194–196] The pneumatic driver inside the device conforms to the heart without sutures and compresses the heart in synchrony with the native heart rhythm.

However, the aforementioned soft robotic devices are targeted for biventricular pacing and have not considered the role of interventricular septum. With left-sided heart failure, congestion can increase the pressure of the diseased LV and thereby shift the movement of the interventricular septum toward the normal right ventricle, increasing the risk of right-sided heart failure.[197] A soft robotic device anchored into the ventricular wall and an interventricular septum was proposed to augment heart function for one-sided heart failure (Figure 8j).[198,199] Two McKibben soft actuators are oriented to be centrally adjacent to a semilunar bracing frame, and the other two actuators are oriented distally on either side of the bracing frame. The ventricle contracts as the soft actuators are inflated (systolic phase; Figure 8j, right), and relaxes as the soft actuators are deflated (diastolic phase; Figure 8j, left). To assist in the recoiling of the ventricle, elasticated recoil bands were used to couple the bracing frame and a ventricular wall anchor (Figure 8k, left). In vivo testing on pig hearts confirmed the efficacy of the elasticated recoil band on augmenting the refilling of the ventricle during the diastolic phase (Figure 8k, right).

3.3. Soft Bioelectronics–Integrated Ablation Therapy

For a diseased heart, electrical impulses originating from cells other than the SA node can compete with the SA node and initiate abnormal contraction (a condition called atrial fibrillation (AF)).[112] One way to treat AF is catheter ablation, in which the catheter is inserted into the heart to ablate arrhythmic source of the heart (Figure 1c, bottom left). Typically, pulmonary veins (PVs) are electrically isolated, preventing abnormal electrical activity from reaching healthy cardiac tissues.[200,201] Previously, AF ablation has largely relied on point-electrode catheter ablation, in which dozens of single points are ablated to form a continuous ablation line without the ability to visually observe the ablated site.[202] Balloon-catheter-based ablation has received attention as a viable alternative to a point-electrode catheter because the inflation of the balloon catheter within the left atrium creates a continuous contact loop with the endocardium. Furthermore, recent advances in balloon-catheter-based ablation have focused on cryoablation,[203,204] RF ablation,[204,205] laser ablation,[206–208] and sensor integration (e.g., temperature,[160,209] contact force,[205,210,211] and flow sensors[212]).

Flexible and stretchable temperature sensors with various shapes have been developed to monitor local temperatures during ablation therapy. The ability to track local temperatures during ablation could provide clinicians with improved efficacy and safety by controlling the time and size of ablation. A microfabricated Ti/Pt (thicknesses: 5/50 nm) thermistor array has been mounted on thin bioresorbable 2D sheets of silk to monitor both RF ablation and cryoablation (**Figure 9**a).[108] Sixteen thermistors were fabricated in a square area with a side length of ≈20 mm, and four of them were used to demonstrate the mapping of local temperatures. The temperature sensors could monitor temperatures as low as ≈–48 °C during cryoablation with dry ice. To overcome 2D sheet that cannot cover the full epicardial surface of the heart, the same number (16) of serpentine Au resistors (width: 20 μm, thickness: 50 nm) were fabricated on an 3D elastic membrane that precisely matches the epicardium of a rabbit heart (Figure 9b, left).[110] When a cautery pen acutely burned a small region of the epicardium, the array could map the localized temperature arising near the point of ablation (Figure 9b, right). Although the coverage of the membrane has been widened to the entire epicardial surface, the spatial density of temperature sensors has become lean. Unlike the aforementioned temperature sensors that monitor the thermal distributions on epicardial surfaces, flexible needle-type temperature sensors have been injected into myocardial tissue for the purpose of monitoring the temperature, thermal conductivity, and volumetric heat capacity at different depths during RF ablation and cryoablation (Figure 9c).[213] Ultrathin geometries minimize the damage to tissue during injection and did not impede cardiac motion. Chronothermographs at three locations across the wall enable the characterization of the thermal energy profiles in the transverse direction during lesion formation. Four key parameters that characterize the shape of a chronothermograph have been extracted, and on the basis of these parameters, transmural and nontransmural lesions could be differentiated.

Another idea in research on ablation therapy is to mount soft bioelectronics directly onto the surface of a balloon-catheter-based system, rendering it multifunctionality. A balloon catheter was instrumented with an array of sensors (ECG, contact pressure, flow, and temperature) and actuators (LEDs and RF ablation electrodes) (Figure 9d).[209] The sensors and actuators were arranged in a mesh network and could withstand tensile strains up to 200% without causing fracture. The contact pressure sensor was insensitive to in-plane forces such as the forces that can occur during inflation and deflation processes but was highly sensitive to normal forces, making it a suitable device for detecting the mechanical forces exerted on the balloon–tissue interface. A thin serpentine layer of Ti/Pt (thicknesses: 5/50 nm) was fabricated for temperature sensing and placed between two pairs of RF ablation electrodes to monitor lesion formation (Figure 9e, left). The pattern of the chronothermograph is consistent with the change in the RF power input (Figure 9e, right). Even though the balloon catheter is designed for endocardial application, the demonstration was conducted on the epicardial surface. Another simple option for contact sensing is an impedance-based sensor, in which a bipolar pair of electrodes measures the shifts in the impedance generated by small amounts of AC (<10 μA; Figure 9f).[214] Since myocardial tissue is about 2–3 times more conductive than blood, the impedance-based contact sensor can be used to confirm contact with cardiac tissue during ablation.

A powerful and clinician-friendly global ablation catheter with the capability of contact, temperature, and intracardiac electrogram sensing has been developed for circumferential PV isolation (Figure 9g, left).[215] The global catheter consists of 16 ribs with 122 Au electrodes, and flexible electronic circuits including temperature sensors are positioned directly beneath

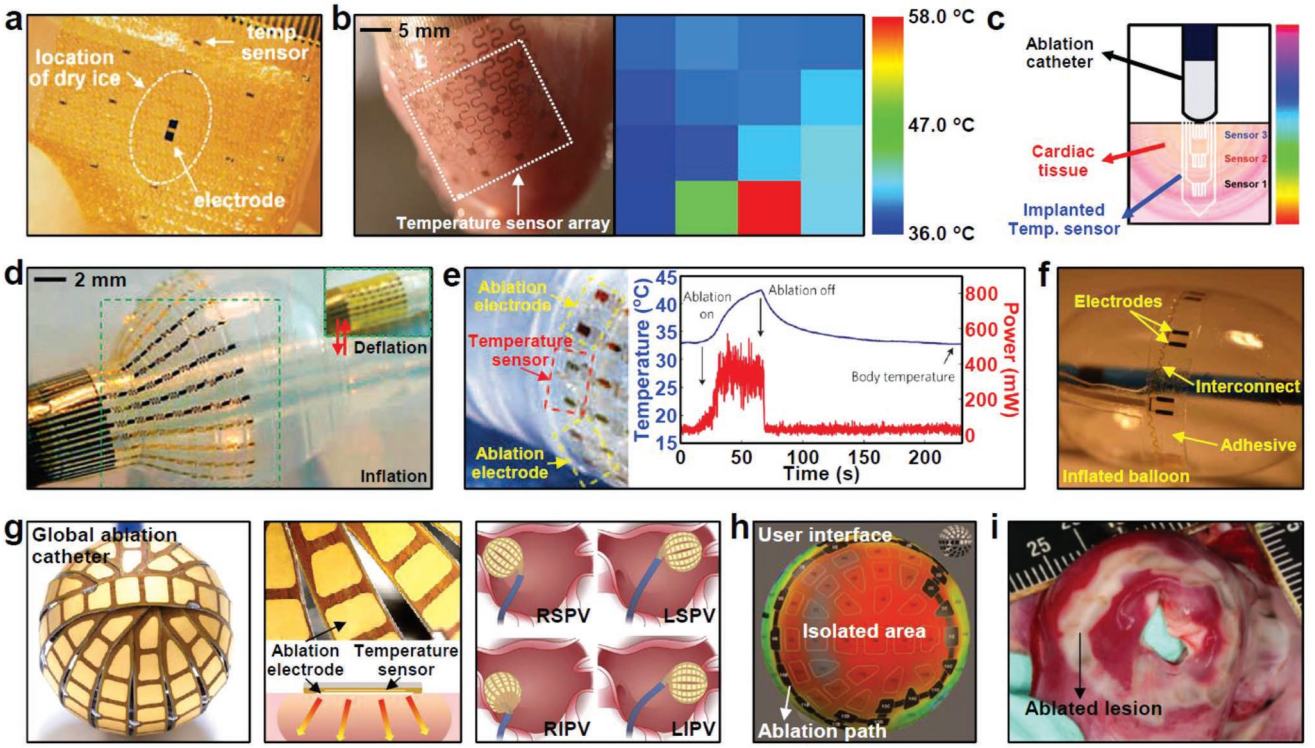

Figure 9. Soft bioelectronics–integrated ablation therapy. a) Optical image of thermistor array fabricated on a bioresorbable 2D sheet of silk. Reproduced with permission.[108] Copyright 2012, National Academy of Sciences. b) Optical image of a 3D-MIM with a temperature sensor array laminated on a rabbit epicardium (left) and a temperature map during ablation with a cautery pen (right). Reproduced with permission.[110] Copyright 2014. Nature Publishing Group. c) Schematic of a flexible needle-type temperature sensor array injected into the endocardial surface. Reproduced with permission.[213] Copyright 2016. Wiley-VCH. d) Optical image of an inflated balloon catheter with an array of sensors and actuators. The inset shows the deflated balloon catheter. Reproduced with permission.[209] Copyright 2011. Nature Publishing Group. e) Magnified optical image of ablation electrodes and temperature sensors laminated on the balloon catheter in (d) (left) and the temperature recorded with changes in the RF ablation (blue) and RF input power (red) (right). Reproduced with permission.[209] Copyright 2011. Nature Publishing Group. f) Optical image of an impedance-based contact sensor laminated on an inflated balloon catheter for tactile sensing. Reproduced with permission.[214] Copyright 2014, Elsevier. g) Optical image of a global ablation catheter consisting of 16 ribs with 122 Au electrodes (left), an optical image (top center) and a schematic showing the side view (bottom center) of Au electrodes with an embedded temperature sensor, and schematics of the global catheter placed at the antrum of each PV (right). Right superior PV (RSPV; top left), left superior PV (LSPV; top right), right inferior PV (RIPV), and left inferior PV (LIPV). Reproduced with permission.[215] Copyright 2017, Wiley-VCH. h) Voltage map, a customized user interface, after complete RIPV isolation with the global catheter in (g). Reproduced with permission.[215] Copyright 2017, Wiley-VCH. i) Optical image of canine endocardium with a PV isolated by the ablation catheter in (g) forming a transmural and contiguous lesion. Reproduced with permission.[215] Copyright 2017, Wiley-VCH.

each Au electrode (Figure 9g, center). The gaps between the ribs allow for blood flow when the catheter is placed at the antrum of a PV for circumferential isolation (Figure 9g, right). The data monitored by 122 electrodes are continuously displayed in a number of maps that show the amount of contact (FLOW map), the electrogram amplitude (voltage map), and the propagation of the activation wave front (WAVE map) (Figure 9h). After confirming conformal contact with the FLOW and voltage maps, the ablation electrodes are selected around the PV. Then, RF energy is delivered to the selected electrodes, in which the temperature sensors automatically control the input power of each electrode to maintain the target temperature. The WAVE map is used to confirm complete PV isolation, in which an activation wave front does not enter the isolated area. In addition, the voltage map shows the decrease in the electrogram amplitude within the ablation path (Figure 9h). In this way, the global catheter could successfully form a continuous and transmural lesion (Figure 9i).

3.4. Soft Bioelectronics–Integrated Stents

The heart muscle, like every other tissue in your body, needs O_2 and nutrients to operate, and coronary arteries—the branches of the aorta—are responsible for supplying O_2-rich blood to the entire heart muscle. When the inner wall of the coronary artery is damaged, fatty plaque consisting of cholesterol and cellular waste products can build on the injured site of a coronary artery. The build-up of plaque narrows the coronary arteries (stenosis) and reduces the supply of O_2-rich blood to the heart muscle. The lack of O_2-rich blood to the heart would eventually lead to a heart attack.

Balloon angioplasty was developed in the 1970s, in which a catheter with a small deflated balloon on its tip is delivered to a narrowed artery and the balloon is inflated to expand the walls of a blocked artery.[216] However, stenosis recurs (restenosis) in about 50% of patients within 6 months after balloon angioplasty.[217,218] To solve this problem, a stent—a

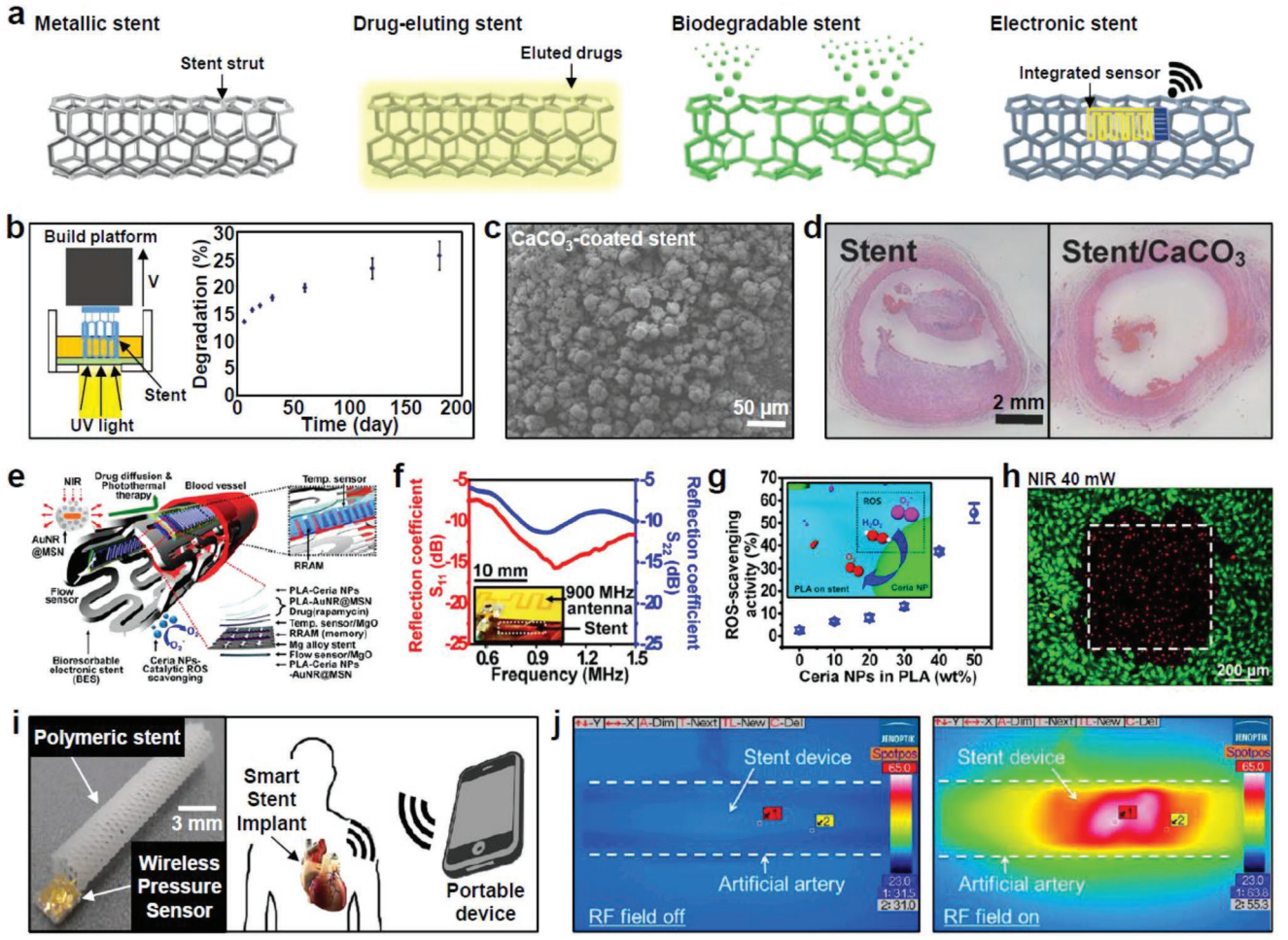

Figure 10. Soft bioelectronics–integrated stents. a) Schematics of metallic (far left), drug-eluting (second left), biodegradable (second right), and electronic stents (far right). b) Schematic showing the 3D printing of a patient-specific biodegradable stent (left) and the degradation profile of 3D-printed on-the-spot stents (right). Reproduced with permission.[233] Copyright 2016, Wiley-VCH. c) SEM image of a stent coated with vaterite-phase $CaCO_3$ crystals. Reproduced with permission.[234] Copyright 2017, Wiley-VCH. d) Histological analysis of blood vessels in rats implanted with a PCL stent (left) and $CaCO_3$-coated PCL stent (right). Reproduced with permission.[234] Copyright 2017, Wiley-VCH. e) Schematic of a bioresorbable electronic stent equipped with flow and temperature sensors (inset), data storage, ceria NPs, and an antiproliferative drug. Reproduced with permission.[239] Copyright 2015, ACS Publications. f) Reflection coefficients of the Mg-based stent antenna in (e) in vivo and a transmitting external antenna (900 MHz). The inset shows an optical image of the experimental setup for wireless power/data transmission. Reproduced with permission.[239] Copyright 2015, ACS Publications. g) ROS scavenging activity of poly(lactic acid) (PLA) films with varying ceria NP concentrations. The inset shows a schematic of the ROS scavenging mechanism of ceria NPs. Reproduced with permission.[239] Copyright 2015, ACS Publications. h) Image of cells on a PLA film dyed with a fluorescent live/dead assay after irradiation with a 40 mW NIR laser. The area inside the whited dashed box was irradiated. Red indicates dead cells, and green indicates live cells. Reproduced with permission.[239] Copyright 2015, ACS Publications. i) Optical image of a polymeric stent integrated with a wireless pressure sensor (left) and schematic of a wireless BP monitoring stent (right). Reproduced with permission.[241] Copyright 2017, IEEE. j) IR image of a stainless-steel stent device expanded inside an artificial artery with (right) and without (left) excitation by RF power. Reproduced with permission.[242] Copyright 2015, Elsevier.

small expandable tubular structure made of metal mesh—is mounted on the balloon catheter (Figure 1c, top left and **Figure 10**a far left).[219] The expanded stent keeps the artery open after removing the balloon catheter. In this respect, coronary stents have revolutionized the field of angioplasty and become the new standard angioplasty procedure.[220] Stent implantation is advantageous in that it does not accompany an abrupt vessel closure, a major complication of balloon angioplasty, and operates well for a long time compared to balloon angioplasty. However, metallic stents cause mechanical damage upon implantation and predispose vascular tissue to neointimal hyperplasia and thrombosis. Although less frequent than balloon angioplasty, when neointimal proliferation becomes worse, the artery can be restenosed (in-stent restenosis).[221,222] Therefore, stent technology has evolved to overcome in-stent restenosis. One of the improvements in stent technology is drug-eluting stents (Figure 10a, second left).[220,223–225] The stent is coated with numerous pharmacological drugs with antiproliferative properties (e.g., actinomycin D, sirolimus, and paclitaxel) that are slowly released to inhibit neointimal proliferation. This allows for local drug application at the precise site and time of injury. Since systemic

release is minimal compared to taking these medicines, the risk of toxicity is reduced.[220] Another approach is to fabricate stents out of biodegradable materials as an alternative to permanent stents, because stents are only needed temporarily and the presence of a stent strut may cause long-term complications such as late thrombosis (Figure 10a, second right).[226–232] There has been a first attempt of the patient-specific customization of biodegradable stents using 3D imaging and 3D printing technology (Figure 10b, left).[233] The manufactured on-the-spot patient-specific stents degraded ≈25% in 6 months (Figure 10b, right). Furthermore, drug-eluting and biodegradable stents are combined by depositing vaterite-phase calcium carbonate ($CaCO_3$) crystals onto a polydopamine-coated polycaprolactone (PCL) stent (Figure, 10c).[234] In acidic environments such as fat-rich plaques, the $CaCO_3$ crystals react with protons to generate CO_2 microbubbles, which prevent restenosis by dissolving locally accumulated plaque. Blood vessels implanted with PCL stents restenosed after 1 month of implantation (Figure 10d, left), whereas blood vessels implanted with $CaCO_3$-coated PCL stents did not accumulate plaque (Figure 10d, right). In addition, the CO_2 microbubbles are strongly echogenic and can serve as a contrast agent, enabling noninvasive ultrasound imaging after stent implantation.

The integration of soft bioelectronics with bioresorbable stent implantation enables the tracking of local hemodynamic changes and active control of advanced therapeutic treatments (Figure 10a. far right).[235–238] Figure 10e shows a bioresorbable electronic stent consisting of bioresorbable (Mg, MgO, SiO_2, Zn, ZnO, and poly(lactic acid)) and bioinert (Mn) materials.[239] The electronic stent is equipped with flow and temperature sensors, data storage (resistive random access memory (RRAM)), ceria nanoparticles (NPs), and an antiproliferative drug (rapamycin). The conductive Mg-based stent strut acts as an antenna for wireless power/data transmission (Figure 10f). A thermoresistive flow sensor operates by measuring changes in the resistance and stores the measured data in the RRAM for further analysis. Ceria NPs catalytically scavenge reactive oxygen species (ROS) near the implantation site to reduce ROS-induced inflammatory responses (Figure 10g). Rapamycin is loaded on a Au nanorod core/mesoporous silica nanoparticle shell (AuNR@MSN), which is responsive to a near-IR laser (wavelength: ≈800 nm) that can penetrate soft tissue. This enables active control over the noninvasive photothermal actuation of drug release.[240] In addition, the near-IR laser activation of AuNR@MSN induces hyperthermia and provides thermal therapy via feedback control with temperature sensing (Figure 10h). To check the BP near the implantation site, a pressure sensor that can be wirelessly monitored via RF waves has been integrated into a biodegradable polymeric stent based on PCL (Figure 10i).[241] Polymeric stents are used because metallic stents can potentially interfere with the RF waves generated by an external coil. The wireless-pressure-sensor-integrated stent can be used to diagnose in-stent restenosis since restenosis changes the local hemodynamics of the implantation site, modifying the local BP. A wireless resonant-heating stent can be a possible solution for treating in-stent restenosis, in which a stainless-steel stent functions as an electrical inductor and an integrated flexible capacitor strip forms a passive resonant circuit. (Figure 10j).[242] The device could provide an increase in the temperature of more than 30 °C using an RF power of 320 mW, which is sufficiently effective for the endohyperthermia therapy of in-stent restenosis.

4. Soft Bioelectronics–Assisted Tissue Engineering

4.1. Cell-Based Cardiac Therapy

Damaged cardiac tissue including ischemic heart diseases does not regenerate or restore by itself.[243,244] To restore the intrinsic function of cardiac tissue, heart transplantation has been the only option.[245] As mentioned earlier, heart transplantation is limited owing to the low availability[246,247] of heart donors and the high risk of immune response.[248,249] Hence, cell-based therapies have gained attention for their capability to treat damaged cardiac tissue.[250–252] Cell therapies for ischemic heart diseases and heart failure have been performed in clinical trials.[253] In most of these clinical trials, cells were directly injected into an infarcted area or the corresponding coronary artery (**Figure 11**a).[254] The intracoronary transplantation of autologous bone marrow cells (BMCs) into patients with acute myocardial infarction has significantly improved left ventricular performance without noticeable side effects. A total of 62 patients have received BMC therapy, and therapeutic follow-up has been performed 3, 12, and 60 months after therapy. The ejection fraction, the percentage of blood leaving the heart during its contraction, was much higher in the BMC group compared to the control group (Figure 11b).[255] In addition, the administration of autologous cardiosphere-derived cells and human mesenchymal stem cells to an infarcted heart has shown therapeutic efficacy.[256] These cells have been administered to subjects via intracoronary infusion and intramyocardial injection.[257–260]

Although cell therapies have shown improvement in left ventricular function,[261] there is no strong evidence that the administered cells have successfully engrafted with the host myocardium.[262,263] The therapeutic effect may have shown by the paracrine effect owing to the low survivability of the injected donor cells.[264,265] Even if the cells have engrafted into the host myocardium, only 0.1 to 10% of the cells continue to survive for more than a few weeks.[255] Moreover, the injection of the cells requires a very large number of cells because most cells are washed away during administration.[266] In order to efficiently and effectively transplant cells, cell sheet technology has been implemented.[267] The cells are cultured on a thermoresponsive polymer in vitro and form into a monolayer sheet of cells (Figure 11c).[268] Cell sheet technology allows a high density of cells to be transplanted only at the target location (Figure 11d).[269]

To overcome the issue of low viability, various types of scaffolds and biomaterials that provide an adequate environment for the transplanted cells in vivo have been developed.[270] Cells are cultured on a scaffold to increase viability during engraftment and to guide cellular behavior such as differentiation.[271,272] Because cardiac cells in vivo are naturally aligned,[273] it is important for the transplanted cells to be aligned in vitro.[32,33] A scaffold comprising nanofibers and encapsulated by a hydrogel

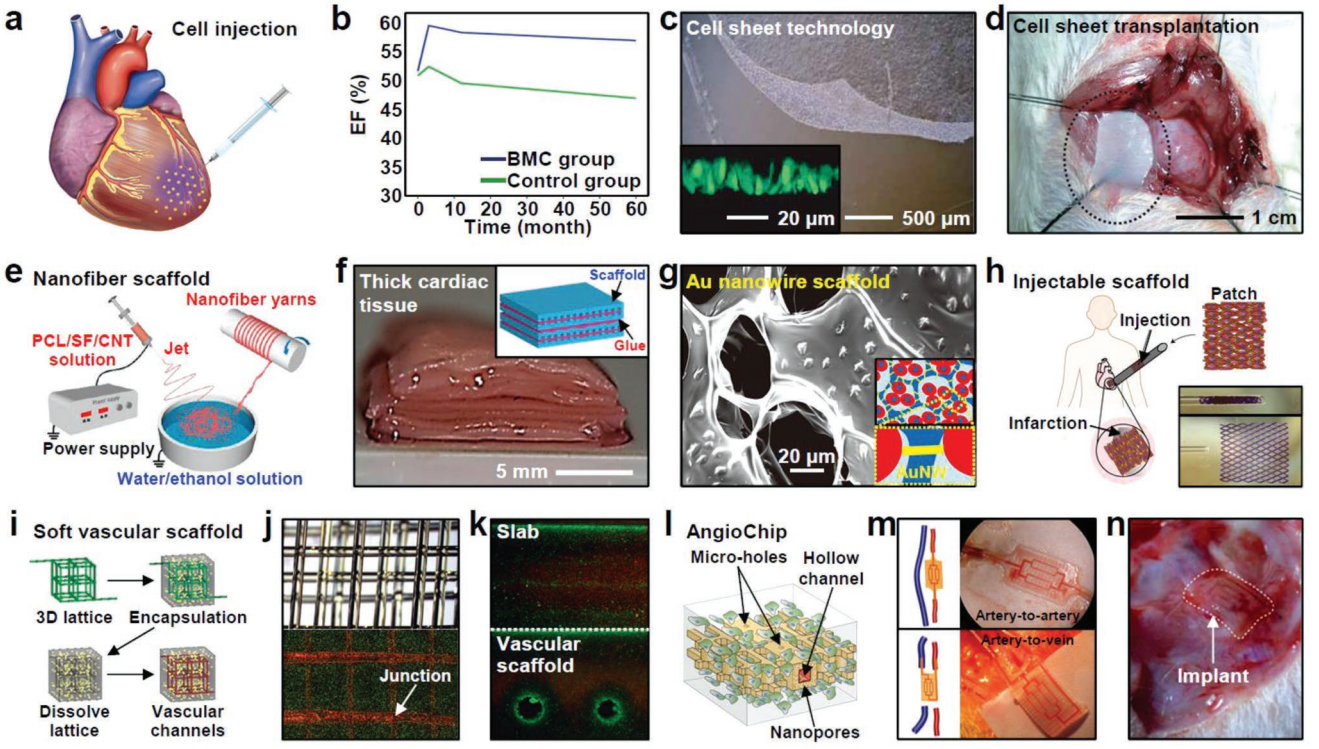

Figure 11. Cell-based cardiac therapy. a) Schematic of cardiac cell therapy by direct injection. Reproduced with permission.[254] Copyright 2017, Elsevier. b) Plot showing the improvement in the ejection fraction (EF) for the BMCs group compared to the control group. Reproduced with permission.[255] Copyright 2009, Elsevier. c) Optical image of a monolayer cell sheet harvested on a thermo-responsive polymer. The inset shows cross-sectional confocal images of the green fluorescent protein (GFP)-expressed monolayer cell sheet after detachment from the polymer. Reproduced with permission.[269] Copyright 2006, Nature Publishing Group. d) Surgical operation of cell sheet transplantation on the infarcted heart of a rat. Reproduced with permission.[269] Copyright 2006, Nature Publishing Group. e) Schematic of nanofiber scaffold fabrication by an electrospinning process and a weaving technique using PCL/SF/CNT solution. Reproduced with permission.[274] Copyright 2017, ACS Publications. f) Optical image of a 5 mm thick tissue construct with assembled albumin scaffold layers. The inset shows a schematic of the thick assembled scaffold. Reproduced with permission.[275] Copyright 2017, National Academy of Sciences. g) SEM image of a AuNW-incorporating cardiac patch. The inset shows a schematic of AuNWs bridging the pores of the alginate hydrogel. Reproduced with permission.[282] Copyright 2011, Nature Publishing Group. h) Schematic of a flexible shape-memory scaffold injected into the heart for minimally invasive delivery. The inset shows an optical image of the shape-memory scaffold before and after injection via a glass pipette. Reproduced with permission.[283] Copyright 2017, Nature Publishing Group. i) Schematic showing the fabrication of vascular channels within the ECMs hydrogel. Reproduced with permission.[289] Copyright 2012, Nature Publishing Group. j) Optical image of the carbohydrate-glass lattice (top) and a fluorescent image of blood vessel junctions (bottom). Reproduced with permission.[289] Copyright 2012, Nature Publishing Group. k) Staining images of the slab gel (top right) and the vascular scaffold (bottom right) with a fluorescent live/dead assay. Reproduced with permission.[289] Copyright 2012, Nature Publishing Group. l) Schematic of biodegradable scaffold with built-in vasculature, AngioChip. Reproduced with permission.[290] Copyright 2016, Nature Publishing Group. m) Schematics (left) and images (right) of the surgical anastomosis of AngioChip cardiac tissue artery-to-artery (top) and artery-to-vein (bottom). Reproduced with permission.[290] Copyright 2016, Nature Publishing Group. n) Optical image of AngioChip implantation on the hind limb of a rat. Reproduced with permission.[290] Copyright 2016, Nature Publishing Group.

mimics a 3D anisotropic environment (Figure 11e).[274] PCL, silk fibroin (SF), and carbon nanotubes (CNTs) were used to fabricate nanofiber yarn by a wet–dry electrospinning process and weaving technique. The addition of CNTs formed an electrically conductive network in the scaffold. The functional engineered cardiac tissue requires a combination of more than one type of cell and should be thick. Furthermore, different types of cells need different culture media and environments. Electrospun albumin fiber scaffolds were laser-printed and assembled together by an extracellular matrix (ECM)-based biological glue, creating a 5 mm thick engineered tissue (Figure 11f).[275] Fibrous layers were fabricated separately into a grooved layer for cardiac cell alignment, channels for endothelial cells, and cages for dexamethasone (DEX) particles and were assembled together before transplantation.

Hydrogels are another popular biomaterial used to fabricate scaffolds because they are high in water content, which is favorable for cell culturing.[276–278] To enhance the cell–cell interaction between cardiac cells that are electrically connected in vivo, hydrogel-based scaffolds are made into a conductive hydrogel by incorporating conducting materials such as PEDOT:PSS,[279] polyaniline,[280] and nanomaterials.[281] The incorporation of Au nanowires (AuNWs) into an alginate hydrogel successfully formed an electrically conductive path between insulating pore walls, thereby increasing the electrical communication between cardiac cells (Figure 11g).[282] The transplantation of these scaffolds requires an invasive surgical procedure, i.e., opening the chest. Recently, a minimally invasive delivery method has been developed, in which cells cultured on a shape-memory scaffold are directly injected to

the infarcted heart. The flexible and elastic scaffold comprises a biodegradable polymer and recovers its initial shape after injection (Figure 11h).[283]

A critical factor for increasing the viability of transplanted cells is to provide vascularization within the scaffolds that supplies O_2 and nutrients,[284,285] especially for thick, 3D-engineered, cardiac tissue.[286] Further, it is important to construct a scaffold bridging the blood vessels because many heart failures are caused by coronary artery blockage. Many engineered scaffolds, however, are not sufficiently sophisticated to accompany vascular constructs.[287,288] 3D sacrificial filaments comprising a carbohydrate-glass lattice serve as a platform for fabricating vascular channels within the scaffold (Figure 11i).[289] The strategy is that these 3D lattice filaments (Figure 11j top) are coated with a thin layer of poly(D-lactide-*co*-glycolide) that allows the carbohydrate glass to dissolve later and flow out. Then, ECM polymers are poured and encapsulate the lattice with the cells. When the filament is dissolved with water, channels are formed within the ECM scaffold. Human umbilical vein endothelial cells (HUVECs) are cultured within the channels to form a vascular construct. Vessels are interconnected via a junction (Figure 11j bottom). The scaffold with the vascular channels shows a much higher cell survivability than a slab without any vascular channels (Figure 11k). Importantly, the viability of the cells residing at the center of the scaffold is significantly higher in the scaffold with vascular channels. Vascular scaffolds made of a soft hydrogel, however, can be unstable during long-term in vivo implantation. Another scaffold made of a biodegradable elastomer, poly(octamethylene maleate (anhydride) citrate), is another promising scaffold for increasing the viability of the transplanted cells and providing a bridge between blood vessels.[290] A scaffold called AngioChip contains hollow channels, microholes, and nanopores for the easy diffusion of gas and nutrients (Figure 11l). Engineered cardiac tissue with AngioChip could connect artery-to-artery and artery-to-vein in vivo by surgical anastomosis, e.g., the rat blood flowing via AngioChip shown in Figure 11m. This cardiac tissue was implanted on a rat's hind limb for a week with direct anastomosis (Figure 11n), and native angiogenesis occurred around the implant.

4.2. Electronics-Integrated Tissue Engineering

Studies on cardiac tissue engineering have focused on constructing cardiac engineered tissue and developing engineered scaffolds, patches, and delivery methods.[291,292] However, most engineered tissues are passive,[293] and their performance regarding the replacement and restoration of an infarcted heart is still limited. The integration of electronics into a scaffold allows cells to be stimulated and monitored before and after the implantation.[32,283] Nevertheless, it is difficult to incorporate rigid electronics into soft and elastic biomaterials.[33] Recent advances in flexible and soft electronics, however, have allowed the fabrication of active scaffolds, in which sensing and stimulation are incorporated within 3D scaffolds.[294,295] Nanoelectronics comprising Si nanowire field-effect transistors (FETs) based on SU-8 polymer backbones have been fabricated on sacrificial layers (**Figure 12**a).[296] This electronic scaffold can be integrated with macroporous ECMs such as electrospun nanofibers (Figure 12b) and alginate hydrogels (Figure 12c, left). Cardiomyocyte is three-dimensionally cultured on this scaffold with a high viability (Figure 12c, right), and the electronic scaffold records the extracellular electrical activity of cells. The frequency of the conductance recording is significantly increased after the treatment of noradrenaline (Figure 12d).

Although nanowire-based FETs are suitable for recording electrical activity with a high SNR, they are poor for performing the electrical stimulation or drug release onto 3D cardiac tissue due to limitations on supplying a current.[296] Hence, another electronic scaffold accompanied with 28 spatially distributed Au electrodes and four electrodes for the controlled release of drugs has been developed.[297,298] The Au electrode array was passivated by SU-8 and encapsulated by electrospun PCL–gelatin fibers to construct a 3D cardiac scaffold that mimics natural ECMs. The engineered cardiac tissue on this electronic scaffold can be constructed (Figure 12e) with sensing and stimulation capabilities. In the active drug release system, two types of electroactive polymers that can store and release either positively or negatively charged proteins have been deposited onto the Au electrodes (Figure 12f, left). DEX is an anti-inflammatory drug that reduces inflammation during implantation. Polypyrrole and DEX were deposited onto the electrode by electropolymerization. The amount of drug released can be modulated by controlling the applied voltage (Figure 12f, right).

One of the major purposes of an electronic scaffold is to monitor and stimulate cardiac tissue during long-term in vivo implantation.[296] Previous electronic scaffolds, however, consisted of nondegradable synthetic materials such as SU-8 or PI, and an additional surgical procedure is inevitable to remove the synthetic scaffold.[293,294] Therefore, an electronic scaffold that can degrade in vivo is needed.[299–301] The Au electrodes were fabricated onto an electrospun albumin scaffold, which serves as a substrate and passivation layer, to construct engineered cardiac tissue (Figure 12g; the inset shows an image of a rolled scaffold).[302] This scaffold can record the electrical activity of cultured cardiac cells and stimulate these cells. To test biodegradability, the scaffold was implanted subcutaneously into an adult rat (Figure 12h, inset). An in vivo degradation test showed that the biomaterial component (albumin) degraded, the inorganic materials (Au) dissociated into small fragments, and the remaining area of the implanted scaffold significantly decreased (Figure 12h).

Engineered cardiac tissue is not only intended to be engrafted in vivo for regenerative medicine; it is also important to create sophisticated engineered cardiac tissue for in vitro testing platforms.[303,304] The availability of in vivo heart organs—especially a human heart—is very limited.[305] Moreover, it is rare to utilize an in vivo organ for testing novel drugs. Nonhuman animal testing may not be effective for studying novel substances for human trials owing to the differences between species. A tissue-scaffold-mimicking 3D nanoelectronic array scaffold enables the 3D mapping of electrophysiology in engineered cardiac tissue (Figure 12I, top left).[306,307] A high-density array of 64 Si nanowire FETs was fabricated and folded to construct a four-layer 3D scaffold. The conductance of the cultured cardiomyocytes at each FET was recorded to monitor the electrical activity, and the results

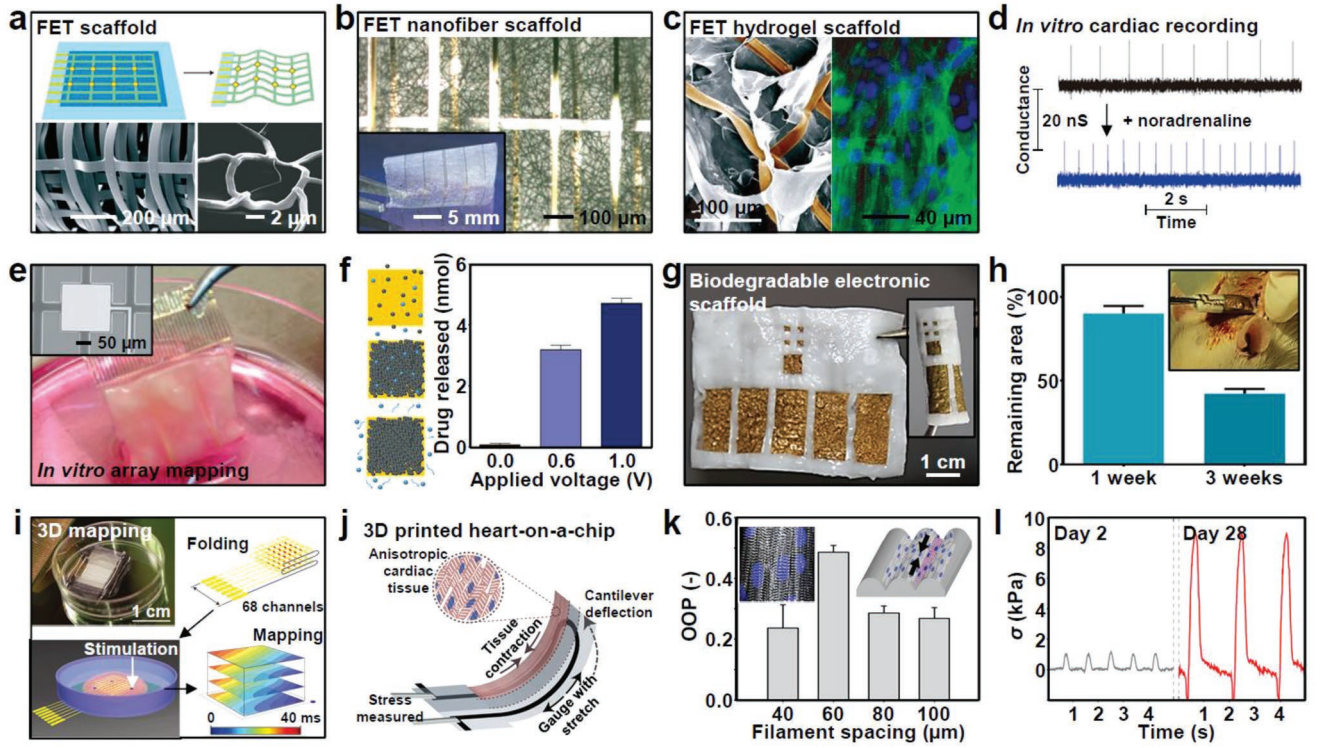

Figure 12. Electronics-integrated tissue engineering. a) Schematic of a Si nanowire FET-integrated macroporous scaffold (top) and SEM images of the FET scaffold (bottom). Reproduced with permission.[296] Copyright 2012, Nature Publishing Group. b) Magnified image of an FET scaffold composed of electrospun nanofibers. The inset shows an optical image of the thin FET scaffold. Reproduced with permission.[296] Copyright 2012, Nature Publishing Group. c) SEM image of an FET scaffold comprising hydrogel (left) and a fluorescence image of the cells cultured on the FET scaffold (right). Reproduced with permission.[296] Copyright 2012, Nature Publishing Group. d) Conductance of the cardiomyocytes recorded by the FET scaffold before (top) and after (bottom) treatment with noradrenaline. Reproduced with permission.[296] Copyright 2012, Nature Publishing Group. e) Optical image of a cardiac patch integrated with an array of electrodes. The inset shows a magnified image of the electrode. Reproduced with permission.[298] Copyright 2016, Nature Publishing Group. f) Controlled drug release system within the electronic cardiac patch in (e): schematic showing the deposition of a drug onto the electrode and the active release of the drug (left) and a plot showing the amount of released drug for different applied voltages (right). Reproduced with permission.[298] Copyright 2016, Nature Publishing Group. g) Optical image of a biodegradable electronic scaffold. The inset shows an optical image of a rolled electronic scaffold. Reproduced with permission.[302] Copyright 2018, Elsevier. h) Biodegradability test of a scaffold. The remaining area of the scaffold was reduced after in vivo implantation for 1 week and 3 weeks. The inset shows an optical image of the partially degraded scaffold removed from the implantation site in vivo. Reproduced with permission.[302] Copyright 2018, Elsevier. i) 3D multilayer electronic scaffold composed of an array of electrodes (top left) and a schematic of scaffold fabrication and 3D mapping. Reproduced with permission.[306] Copyright 2016, Nature Publishing Group. j) 3D-printed heart-on-a-chip recording the contractile stress of cardiac cells by the deflection of a cantilever and a strain gauge sensor. Reproduced with permission.[309] Copyright 2016, Nature Publishing Group. k) Plot showing the sarcomere orientation order parameter (OOP) for different filament spacings. The insets show cellular alignments of cardiac cells on PDMS grooves with a spacing of 60 μm. Reproduced with permission.[309] Copyright 2016, Nature Publishing Group. l) Plots showing the contractile stress of the cardiomyocytes cultured on the 3D-printed heart-on-a-chip in j). Reproduced with permission.[309] Copyright 2016, Nature Publishing Group.

were rendered into 3D isochronal maps. Moreover, the 3D array of FETs recorded the action potential propagation of cardiomyocytes induced by localized electrical stimulation (Figure 12i).

An advanced in vitro electronic scaffold has been developed by easy and fast fabrication using 3D printer.[308,309] The microphysiological activity of cardiac cells could be monitored by a cantilever and soft strain gauge sensors (Figure 12j). A thermoplastic polyurethane (TPU) ink has been utilized for the substrate of the cantilever for free deflection. The strain gauge sensors are also made of TPU with the addition of carbon black NPs. PDMS grooves were fabricated to guide cardiac cells into a uniaxial orientation. The highest percentage of cellular alignment could be achieved with a filament spacing of 60 μm, and the orientation was quantified into a sarcomere orientation order parameter (Figure 12k). The systole and diastole of cardiac cells actuate the deflection of the cantilever. Then, the strain gauge sensor quantitatively measures the tissue contractile stresses in vitro (Figure 12l). The integration of flexible and soft electronics with a facile fabrication method enables the physiological activity monitoring of cardiac cell in vitro for long-term functional studies.

5. Conclusion

Heart-related diseases, both acute and chronic, have received a considerable amount of attention owing to their life-threatening

effect on the human body and have opened up extensive research fields regarding monitoring and therapy. Among the various research fields, soft bioelectronics and tissue engineering have shown outstanding advancements. Wearable and implantable soft bioelectronics have become deeply involved in biomedical applications because of their diverse advantages including multifunctional characteristics, conformal contacts, flexible and stretchable properties, and biocompatible interfaces. Advancements in the electrode designs, materials, and structures of wearable devices have enabled the real-time detection of minute changes in physiological signals, including the ECG and blood oxygen saturation. For biosignals that require a high precision, such as the BP and epicardial mapping, implantable soft bioelectronic devices have been demonstrated to directly measure signals from the targets. Epicardial mapping devices with various forms (i.e., 2D sheets, sleeves, and meshes) conform to the epicardial surface, enabling real-time spatiotemporal mapping.

In addition, soft bioelectronic devices could improve conventional biomedical therapies such as pacing, defibrillation, mechanical supporting, ablation, and stenting. i) For pacemakers, TENGs, PENGs, and solar-power and wireless power transmission provide unlimited battery life. ii) For defibrillation, 3D-MIMs and serpentine meshes conform to ventricles to deliver an electrical shock efficiently. iii) For mechanical support, the previously passive mechanical support devices became active and effective for assisting the heart in synchrony with the native heartbeat. iv) For ablation therapy, temperature sensors have been integrated with multielectrode RF ablation electrodes to monitor and provide feedback-control RF ablation. v) For stents, soft electronic devices have been integrated into biodegradable stents to monitor the healing process and deliver therapeutic drugs.

Meanwhile, tissue engineering has been extensively studied because of its unique capability to fundamentally restore damaged tissue. In particular, engineered scaffolds have been studied to provide a sufficient cell culturing environment that facilitates cells to behave like native cardiac tissue and increases the viability of the engrafted cells in vivo. Moreover, the integration of flexible and soft electronics has enabled active scaffolds to be realized, which monitor and stimulate cells and release drugs in a controlled manner. Thus, the electrophysiological activity of implanted cells can be monitored in vivo. In addition, flexible electronics provide the capability to three-dimensionally map the activity of engineered cardiac tissue in vitro and serve as a platform for in vitro drug testing. Consequently, continued efforts to develop multifunctional and effective treatment devices by taking advantage of soft bioelectronics and tissue engineering hold great promise for managing cardiac health.

Acknowledgements

Y.J.H., H.J., and K.W.C. contributed equally to this work. This work was supported by Korean IBS-R006-A1 (D.-H. Kim group) and US Office of Naval Research (ONR) under Grant No. N00014-16-1-2044 (N. Lu group). Y.J.H. acknowledges NRF (National Research Foundation of Korea) Grant funded by Korean Government (NRF-2017H1A2A1043976-Global Ph.D. Fellowship Program).

Conflict of Interest

The authors declare no conflict of interest.

Keywords

cardiovascular healthcare, device-assisted cell therapy, flexible electronics, implantable device, wearable device

Received: November 20, 2018
Revised: January 18, 2019
Published online:

[1] J. Wu, M. Dong, S. Santos, C. Rigatto, Y. Liu, F. Lin, *Sensors* **2017**, *17*, 2934.
[2] J.-J. Nie, B. Qiao, S. Duan, C. Xu, B. Chen, W. Hao, B. Yu, Y. Li, J. Du, F.-J. Xu, *Adv. Mater.* **2018**, *30*, 1801570.
[3] Y. Khan, A. E. Ostfeld, C. M. Lochner, A. Pierre, A. C. Arias, *Adv. Mater.* **2016**, *28*, 4373.
[4] I. You, B. Kim, J. Park, K. Koh, S. Shin, S. Jung, U. Jeong, *Adv. Mater.* **2016**, *28*, 6359.
[5] J. H. Koo, S. Jeong, H. J. Shim, D. Son, J. Kim, D. C. Kim, S. Choi, J.-I. Hong, D.-H. Kim, *ACS Nano* **2017**, *11*, 10032.
[6] M. K. Choi, O. K. Park, C. Choi, S. Qiao, R. Ghaffari, J. Kim, D. J. Lee, M. Kim, W. Hyun, S. J. Kim, H. J. Hwang, S.-H. Kwon, T. Hyeon, N. Lu, D.-H. Kim, *Adv. Healthcare Mater.* **2016**, *5*, 80.
[7] J. Kim, D. Son, M. Lee, C. Song, J.-K. Song, J. H. Koo, D. J. Lee, H. J. Shim, J. H. Kim, M. Lee, T. Hyeon, D.-H. Kim, *Sci. Adv.* **2016**, *2*, e1501101.
[8] Y. J. Hong, H. Lee, J. Kim, M. Lee, H. J. Choi, T. Hyeon, D.-H. Kim, *Adv. Funct. Mater.* **2018**, *28*, 1805754.
[9] P. J. Blankestijn, M. L. Bots, *Nat. Rev. Nephrol.* **2017**, *13*, 725.
[10] D. Son, J. H. Koo, J.-K. Song, J. Kim, M. Lee, H. J. Shim, M. Park, M. Lee, J. H. Kim, D.-H. Kim, *ACS Nano* **2015**, *9*, 5585.
[11] H. Lee, C. Song, Y. S. Hong, M. S. Kim, H. R. Cho, T. Kang, K. Shin, S. H. Choi, T. Hyeon, D.-H. Kim, *Sci. Adv.* **2017**, *3*, e1601314.
[12] M. K. Choi, J. Yang, K. Kang, D. C. Kim, C. Choi, C. Park, S. J. Kim, S. I. Chae, T.-H. Kim, J. H. Kim, T. Hyeon, D.-H. Kim, *Nat. Commun.* **2015**, *6*, 7149.
[13] Y. Lee, J. Kim, J. H. Koo, T.-H. Kim, D.-H. Kim, *Korean J. Chem. Eng.* **2018**, *35*, 1.
[14] S. Choi, H. Lee, R. Ghaffari, T. Hyeon, D.-H. Kim, *Adv. Mater.* **2016**, *28*, 4203.
[15] Y. Lee, J. Kim, H. Joo, M. S. Raj, R. Ghaffari, D.-H. Kim, *Adv. Mater. Technol.* **2017**, *2*, 1700053.
[16] J. Zhu, M. Dexheimer, H. Cheng, *npj Flexible Electron.* **2017**, *1*, 8.
[17] H. Lee, Y. J. Hong, S. Baik, T. Hyeon, D.-H. Kim, *Adv. Healthcare Mater.* **2018**, *7*, 1701150.
[18] M. K. Choi, I. Park, D. C. Kim, E. Joh, O. K. Park, J. Kim, M. Kim, C. Choi, J. Yang, K. W. Cho, J.-H. Hwang, J.-M. Nam, T. Hyeon, J. H. Kim, D.-H. Kim, *Adv. Funct. Mater.* **2015**, *25*, 7109.
[19] J.-K. Song, D. Son, J. Kim, Y. J. Yoo, G. J. Lee, L. Wang, M. K. Choi, J. Yang, M. Lee, K. Do, J. H. Koo, N. Lu, J. H. Kim, T. Hyeon, Y. M. Song, D.-H. Kim, *Adv. Funct. Mater.* **2017**, *27*, 1605286.
[20] C. Choi, M. K. Choi, S. Liu, M. S. Kim, O. K. Park, C. Im, J. Kim, X. Qin, G. J. Lee, K. W. Cho, M. Kim, E. Joh, J. Lee, D. Son, S.-H. Kwon, N. L. Jeon, Y. M. Song, N. Lu, D.-H. Kim, *Nat. Commun.* **2017**, *8*, 1664.
[21] J. Lee, B. Yoo, H. Lee, G. D. Cha, H.-S. Lee, Y. Cho, S. Y. Kim, H. Seo, W. Lee, D. Son, M. Kang, H. M. Kim, Y. I. Park, T. Hyeon, D.-H. Kim, *Adv. Mater.* **2017**, *29*, 1603169.

[22] J. Yang, M. K. Choi, D.-H. Kim, T. Hyeon, *Adv. Mater.* **2016**, *28*, 1176.
[23] S. Choi, J. Park, W. Hyun, J. Kim, J. Kim, Y. B. Lee, C. Song, H. J. Hwang, J. H. Kim, T. Hyeon, D.-H. Kim, *ACS Nano* **2015**, *9*, 6626.
[24] S. Jung, J. H. Kim, J. Kim, S. Choi, J. Lee, I. Park, T. Hyeon, D.-H. Kim, *Adv. Mater.* **2014**, *26*, 4825.
[25] M. Park, K. Do, J. Kim, D. Son, J. H. Koo, J. Park, J.-K. Song, J. H. Kim, M. Lee, T. Hyeon, D.-H. Kim, *Adv. Healthcare Mater.* **2015**, *4*, 992.
[26] H. Lee, Y. Lee, C. Song, H. R. Cho, R. Ghaffari, T. K. Choi, K. H. Kim, Y. B. Lee, D. Ling, H. Lee, S. J. Yu, S. H. Choi, T. Hyeon, D.-H. Kim, *Nat. Commun.* **2015**, *6*, 10059.
[27] S.-K. Kang, J. Koo, Y. K. Lee, J. A. Rogers, *Acc. Chem. Res.* **2018**, *51*, 988.
[28] J. Kim, H. J. Shim, J. Yang, M. K. Choi, D. C. Kim, J. Kim, T. Hyeon, D.-H. Kim, *Adv. Mater.* **2017**, *29*, 1700217.
[29] H. Wu, W. Gao, Z. Yin, *Adv. Healthcare Mater.* **2017**, *6*, 1700017.
[30] J. R. Venugopal, M. P. Prabhakaran, S. Mukherjee, R. Ravichandran, K. Dan, S. Ramakrishna, *J. R. Soc., Interface* **2012**, *9*, 1.
[31] R. Feiner, T. Dvir, *Nat. Rev. Mater.* **2017**, *3*, 17076.
[32] S. J. Kim, H. R. Cho, K. W. Cho, S. Qiao, J. S. Rhim, M. Soh, T. Kim, M. K. Choi, C. Choi, I. K. Park, N. S. Hwang, T. Hyeon, S. H. Choi, N. Lu, D.-H. Kim, *ACS Nano* **2015**, *9*, 2677.
[33] S. J. Kim, K. W. Cho, H. R. Cho, L. Wang, S. Y. Park, S. E. Lee, T. Hyeon, N. Lu, S. H. Choi, D.-H. Kim, *Adv. Funct. Mater.* **2016**, *26*, 3207.
[34] S. Savonitto, D. Ardissino, C. B. Granger, G. Morando, M. D. Prando, A. Mafrici, C. Cavallini, G. Melandri, T. D. Thompson, A. Vahanian, E. M. Ohman, R. M. Califf, F. Van de Werf, E. J. Topol, *JAMA, J. Am. Med. Assoc.* **1999**, *281*, 707.
[35] S. P. Lee, G. Ha, D. E. Wright, Y. Ma, E. Sen-Gupta, N. R. Haubrich, P. C. Branche, W. Li, G. L. Huppert, M. Johnson, H. B. Mutlu, K. Li, N. Sheth, J. A. Wright, Y. Huang, M. Mansour, J. A. Rogers, R. Ghaffari, *npj Digital Med.* **2018**, *1*, 2.
[36] J. Heikenfeld, A. Jajack, J. Rogers, P. Gutruf, L. Tian, T. Pan, R. Li, M. Khine, J. Kim, J. Wang, J. Kim, *Lab Chip* **2018**, *18*, 217.
[37] D.-H. Kim, N. Lu, R. Ma, Y.-S. Kim, R.-H. Kim, S. Wang, J. Wu, S. M. T. Won, H. A. Islam, K. J. Yu, T.-I. Kim, R. Chowdhury, M. Ying, L. Xu, M. Li, H.-J. Chung, H. Keum, M. McCormick, P. Liu, Y.-W. Zhang, F. G. Omenetto, Y. Huang, T. Coleman, J. A. Rogers, *Science* **2011**, *333*, 838.
[38] W.-H. Yeo, Y.-S. Kim, J. Lee, A. Ameen, L. Shi, M. Li, S. Wang, R. Ma, S. H. Jin, Z. Kang, Y. Huang, J. A. Rogers, *Adv. Mater.* **2013**, *25*, 2773.
[39] M. Ying, A. P. Bonifas, N. Lu, Y. Su, R. Li, H. Cheng, A. Ameen, Y. Huang, J. A. Rogers, *Nanotechnology* **2012**, *23*, 344004.
[40] X. Huang, Y. Liu, H. Cheng, W.-J. Shin, J. A. Fan, Z. Liu, C.-J. Lu, G.-W. Kong, K. Chen, D. Patnaik, S.-H. Lee, S. Hage-Ali, Y. Huang, J. A. Rogers, *Adv. Funct. Mater.* **2014**, *24*, 3846.
[41] J. Kim, A. Banks, H. Cheng, Z. Xie, S. Xu, K.-I. Jang, J. W. Lee, Z. Liu, P. Gutruf, X. Huang, P. Wei, F. Liu, K. Li, M. Dalal, R. Ghaffari, X. Feng, Y. Huang, S. Gupta, U. Paik, J. A. Rogers, *Small* **2015**, *11*, 906.
[42] S. Lim, D. Son, J. Kim, Y. B. Lee, J.-K. Song, S. Choi, D. J. Lee, J. H. Kim, M. Lee, T. Hyeon, D.-H. Kim, *Adv. Funct. Mater.* **2015**, *25*, 375.
[43] S. Yang, Y.-C. Chen, L. Nicolini, P. Pasupathy, J. Sacks, B. Su, R. Yang, D. Sanchez, Y.-F. Chang, P. Wang, D. Schnyer, D. Neikirk, N. Lu, *Adv. Mater.* **2015**, *27*, 6423.
[44] Y. Wang, Y. Qiu, S. K. Ameri, H. Jang, Z. Dai, Y. Huang, N. Lu, *npj Flexible Electron.* **2018**, *2*, 6.
[45] S. Yang, E. Ng, N. Lu, *Extreme Mech. Lett.* **2015**, *2*, 37.
[46] H. Jeong, T. Ha, I. A. Kuang, L. Shen, Z. Dai, N. Sun, N. Lu, presented at *39th Annu. Int. Conf. of IEEE Eng. Med. Biol. Soc.*, Seogwipo, South Korea, July **2017**.
[47] S. K. Ameri, M. Kim, I. A. Kuang, W. K. Perera, M. Alshiekh, H. Jeong, U. Topcu, D. Akinwande, N. Lu, *npj 2D Mater. Appl.* **2018**, *2*, 19.
[48] P. Gutruf, V. Krishnamurthi, A. Vázquez-Guardado, Z. Xie, A. Banks, C.-J. Su, Y. Xu, C. R. Haney, E. A. Waters, I. Kandela, S. R. Krishnan, T. Ray, J. P. Leshock, Y. Huang, D. Chanda, J. A. Rogers, *Nat. Electron.* **2018**, *1*, 652.
[49] S. B. Kim, K. Lee, M. S. Raj, B. Lee, J. T. Reeder, J. Koo, A. Hourlier-Fargette, A. J. Bandodkar, S. M. Won, Y. Sekine, J. Choi, Y. Zhang, J. Yoon, B. H. Kim, Y. Yun, S. Lee, J. Shin, J. Kim, R. Ghaffari, J. A. Rogers, *Small* **2018**, *14*, 1802876.
[50] S. R. Krishnan, C.-J. Su, Z. Xie, M. Patel, S. R. Madhvapathy, Y. Xu, J. Freudman, B. Ng, S. Y. Heo, H. Wang, T. R. Ray, J. Leshock, I. Stankiewicz, X. Feng, Y. Huang, P. Gutruf, J. A. Rogers, *Small* **2018**, *14*, 1803192.
[51] A. Miyamoto, S. Lee, N. F. Cooray, S. Lee, M. Mori, N. Matsuhisa, H. Jin, L. Yoda, T. Yokota, A. Itoh, M. Sekino, H. Kawasaki, T. Ebihara, M. Amagai, T. Someya, *Nat. Nanotechnol.* **2017**, *12*, 907.
[52] Z. Cui, Y. Han, Q. Huang, J. Dong, Y. Zhu, *Nanoscale* **2018**, *10*, 6806.
[53] D. Son, J. Kang, O. Vardoulis, Y. Kim, N. Matsuhisa, J. Y. Oh, J. W. F. To, J. Mun, T. Katsumata, Y. Liu, A. F. McGuire, M. Krason, F. Molina-Lopez, J. Ham, U. Kraft, Y. Lee, Y. Yun, J. B.-H. Tok, Z. Bao, *Nat. Nanotechnol.* **2018**, *13*, 1057.
[54] S. K. Ameri, R. Ho, H. Jang, L. Tao, Y. Wang, L. Wang, D. M. Schnyer, D. Akinwande, N. Lu, *ACS Nano* **2017**, *11*, 7634.
[55] L. M. Ferrari, S. Sudha, S. Tarantino, R. Esposti, F. Bolzoni, P. Cavallari, C. Cipriani, V. Mattoli, F. Greco, *Adv. Sci.* **2018**, *5*, 1700771.
[56] G. S. Jeong, D.-H. Baek, H. C. Jung, J. H. Song, J. H. Moon, S. W. Hong, I. Y. Kim, S.-H. Lee, *Nat. Commun.* **2012**, *3*, 977.
[57] C. M. Boutry, A. Nguyen, Q. O. Lawal, A. Chortos, S. Rondeau-Gagne, Z. Bao, *Adv. Mater.* **2015**, *27*, 6954.
[58] T. Kim, J. Park, J. Sohn, D. Cho, S. Jeon, *ACS Nano* **2016**, *10*, 4770.
[59] M. K. Yapici, T. Alkhidir, Y. A. Samad, K. Liao, *Sens. Actuators, B* **2015**, *221*, 1469.
[60] P. M. Barrett, R. Komatireddy, S. Haaser, S. Topol, J. Sheard, J. Encinas, A. J. Fought, E. J. Topol, *Am. J. Med.* **2014**, *127*, 95.e11.
[61] E. Fung, M.-R. Jarvelin, R. N. Doshi, J. S. Shinbane, S. K. Carlson, L. P. Grazette, P. M. Chang, R. S. Sangha, H. V. Huikuri, N. S. Peters, *Front. Physiol.* **2015**, *6*, 149.
[62] L. Lonini, N. Shawen, R. Ghaffari, J. Rogers, A. Jayarman, presented at *Proc. 2017 ACM Int. Joint Conf. Pervasive and Ubiquitous Comput. and Proc. 2017 ACM Int. Symp. Wearable Comput.*, Maui, USA, September **2017**.
[63] https://www.mc10inc.com/our-story#company-overview (accessed: February 2019).
[64] Y. Khan, M. Garg, Q. Gui, M. Schadt, A. Gaikwad, D. Han, N. A. D. Yamamoto, P. Hart, R. Welte, W. Wilson, S. Czarnecki, M. Poliks, Z. Jin, K. Ghose, F. Egitto, J. Turner, A. C. Arias, *Adv. Funct. Mater.* **2016**, *26*, 8764.
[65] P. Shyamkumar, P. Rai, S. Oh, M. Ramasamy, R. E. Harbaugh, V. Varadan, *Electronics* **2014**, *3*, 504.
[66] P. Rai, S. Oh, P. Shyamkumar, M. Ramasamy, R. E. Harbaugh, V. K. Varadan, *J. Electrochem. Soc.* **2014**, *161*, B3116.
[67] K.-I. Jang, K. Li, H. U. Chung, S. Xu, H. N. Jung, Y. Yang, J. W. Kwak, H. H. Jung, J. Song, C. Yang, A. Wang, Z. Liu, J. Y. Lee, B. H. Kim, J.-H. Kim, J. Lee, Y. Yu, B. J. Kim, H. Jang, K. J. Yu, J. Kim, J. W. Lee, J.-W. Jeong, Y. M. Song, Y. Huang, Y. Zhang, J. A. Rogers, *Nat. Commun.* **2017**, *8*, 15894.

[68] Y. Yamamoto, S. Harada, D. Yamamoto, W. Honda, T. Arie, S. Akita, K. Takei, *Sci. Adv.* **2016**, *2*, e1601473.
[69] D. Yamamoto, S. Nakata, K. Kanao, T. Arie, S. Akita, K. Takei, *Adv. Mater. Technol.* **2017**, *2*, 1700057.
[70] Y. Liu, J. J. S. Norton, R. Qazi, Z. Zou, K. R. Ammann, H. Liu, L. Yan, P. L. Tran, K.-I. Jang, J. W. Lee, D. Zhang, K. A. Kilian, S. H. Jung, T. Bretl, J. Xiao, M. J. Slepian, Y. Huang, J.-W. Jeong, J. A. Rogers, *Sci. Adv.* **2016**, *2*, e1601185.
[71] Z. Huang, Y. Hao, Y. Li, H. Hu, C. Wang, A. Nomoto, T. Pan, Y. Gu, Y. Chen, T. Zhang, W. Li, Y. Lei, N. Kim, C. Wang, L. Zhang, J. W. Ward, A. Maralani, X. Li, M. F. Durstock, A. Pisano, Y. Lin, S. Xu, *Nat. Electron.* **2018**, *1*, 473.
[72] S. Xu, Y. Zhang, L. Jia, K. E. Mathewson, K.-I. Jang, J. Kim, H. Fu, X. Huang, P. Chava, R. Wang, S. Bhole, L. Wang, Y. J. Na, Y. Guan, M. Flavin, Z. Han, Y. Huang, J. A. Rogers, *Science* **2014**, *344*, 70.
[73] C. M. Lochner, Y. Khan, A. Pierre, A. C. Arias, *Nat. Commun.* **2014**, *5*, 5745.
[74] J. G. Webster, *Design of Pulse Oximeters*, CRC Press, Boca Raton, FL, USA **1997**.
[75] R. Ortega, C. J. Hansen, K. Elterman, A. Woo, *N. Engl. J. Med.* **2011**, *364*, e33.
[76] T. Tamura, Y. Maeda, M. Sekine, M. Yoshida, *Electronics* **2014**, *3*, 282.
[77] T. Yokota, P. Zalar, M. Kaltenbrunner, H. Jinno, N. Matsuhisa, H. Kitanosako, Y. Tachibana, W. Yukita, M. Koizumi, T. Someya, *Sci. Adv.* **2016**, *2*, e1501856.
[78] D. Han, Y. Khan, J. Ting, S. M. King, N. Yaacobi-Gross, M. J. Humphries, C. J. Newsome, A. C. Arias, *Adv. Mater.* **2017**, *29*, 1606206.
[79] J. Kim, P. Gutruf, A. M. Chiarelli, S. Y. Heo, K. Cho, Z. Xie, A. Banks, S. Han, K.-I. Jang, J. W. Lee, K. T. Lee, X. Feng, Y. Huang, M. Fabiani, G. Gratton, U. Paik, J. A. Rogers, *Adv. Funct. Mater.* **2017**, *27*, 1604373.
[80] H. Li, Y. Xu, X. Li, Y. Chen, Y. Jiang, C. Zhang, B. Lu, J. Wang, Y. Ma, Y. Chen, Y. Huang, M. Ding, H. Su, G. Song, Y. Luo, X. Feng, *Adv. Healthcare Mater.* **2017**, *6*, 1601013.
[81] J. H. Koo, D. C. Kim, H. J. Shim, T.-H. Kim, D.-H. Kim, *Adv. Funct. Mater.* **2018**, *28*, 1801834.
[82] K.-I. Jang, S. Y. Han, S. Xu, K. E. Mathewson, Y. Zhang, J.-W. Jeong, G.-T. Kim, R. C. Webb, J. W. Lee, T. J. Dawidczyk, R. H. Kim, Y. M. Song, W.-H. Yeo, S. Kim, H. Cheng, S. I. Rhee, J. Chung, B. Kim, H. U. Chung, D. Lee, Y. Yang, M. Cho, J. G. Gaspar, R. Carbonari, M. Fabiani, G. Gratton, Y. Huang, J. A. Rogers, *Nat. Commun.* **2014**, *5*, 4779.
[83] J. Kim, G. A. Salvatore, H. Araki, A. M. Chiarelli, Z. Xie, A. Banks, X. Sheng, Y. Liu, J. W. Lee, K.-I. Jang, S. Y. Heo, K. Cho, H. Luo, B. Zimmerman, J. Kim, L. Yan, X. Feng, S. Xu, M. Fabiani, G. Gratton, Y. Huang, U. Paik, J. A. Rogers, *Sci. Adv.* **2016**, *2*, e1600418.
[84] A. K. Bansal, S. Hou, O. Kulyk, E. M. Bowman, I. D. Samuel, *Adv. Mater.* **2015**, *27*, 7638.
[85] J. G. Webster, *Medical Instrumentation: Application and Design, 4th Edition*, Wiley, USA **2009**.
[86] A. Kumar, R. Anel, E. Bunnell, K. Habet, S. Zanotti, S. Marshall, A. Neumann, A. Ali, M. Cheang, C. Kavinsky, J. E. Parrillo, *Crit. Care Med.* **2004**, *32*, 691.
[87] C. Wang, X. Li, H. Hu, L. Zhang, Z. Huang, M. Lin, Z. Zhang, Z. Yin, B. Huang, H. Gong, S. Bhaskaran, Y. Gu, M. Makihata, Y. Guo, Y. Lei, Y. Chen, C. Wang, Y. Li, T. Zhang, Z. Chen, A. P. Pisano, L. Zhang, Q. Zhou, S. Xu, *Nat. Biomed. Eng.* **2018**, *2*, 687.
[88] O. H. Murphy, M. R. Bahmanyar, A. Borghi, C. N. McLeod, M. Navaratnarajah, M. H. Yacoub, C. Toumazou, *Biomed. Microdevices* **2013**, *15*, 737.
[89] Y. Ma, Q. Zheng, Y. Liu, B. Shi, X. Xue, W. Ji, Z. Liu, Y. Jin, Y. Zou, Z. An, W. Zhang, X. Wang, W. Jiang, Z. Xu, Z. L. Wang, Z. Li, H. Zhang, *Nano Lett.* **2016**, *16*, 6042.
[90] J. Park, S. Choi, A. H. Janardhan, S.-Y. Lee, S. Raut, J. Soares, K. Shin, S. TYang, C.-H. Lee, K.-W. Kang, H. R. Cho, S. J. Kim, P. H. Seo, W. S. H. Jung, H.-J. Lee, N. Lee, S. H. Choi, M. Sacks, N. Lu, M. E. Josephson, T. Hyeon, D.-H. Kim, H. J. Hwang, *Sci. Transl. Med.* **2016**, *8*, 344ra86.
[91] P. Cong, N. Chaimanonart, W. H. Ko, D. J. Young, *IEEE J. Solid-State Circuits* **2009**, *44*, 3631.
[92] P. Cong, N. Chaimanonart, W. H. Ko, D. J. Young, presented at *IEEE Int. Solid-State Circuits Conf.*, San Francisco, USA, February **2009**.
[93] P. Cong, W. H. Ko, D. J. Young, *IEEE Sens. J.* **2010**, *10*, 243.
[94] P. Bingger, M. Zens, P. Woias, *Biomed. Microdevices* **2012**, *14*, 573.
[95] N. J. Cleven, J. A. Muntjes, H. Fassbender, U. Urban, M. Gortz, H. Vogt, M. Grafe, T. Gottsche, T. Penzkofer, T. Schmitz-Rode, W. Mokwa, *IEEE Trans. Biomed. Eng.* **2012**, *59*, 3124.
[96] Y. Su, Z. Liu, L. Xu, *Adv. Healthcare Mater.* **2016**, *5*, 889.
[97] J. Penaz, presented at *Digest of the 10th Int. Conf. Med. Biol. Eng.*, Dresden, Germany, August **1973**.
[98] C. Dagdeviren, Y. Su, P. Joe, R. Yona, Y. Liu, Y.-S. Kim, Y. Huang, A. R. Damadoran, J. Xia, L. W. Martin, Y. Huang, J. A. Rogers, *Nat. Commun.* **2014**, *5*, 4496.
[99] G. L. Pressman, P. M. Newgard, *IRE Trans. Bio-Med. Electron.* **1963**, *10*, 73.
[100] G. Ogedegbe, T. Pickering, *Cardiol. Clin.* **2010**, *28*, 571.
[101] A. Avolio, *Hypertension* **2008**, *51*, 1470.
[102] C. M. McEniery, Yasmin, B. McDonnell, M. Munnery, S. M. Wallace, C. V. Rowe, J. R. Cockcroft, I. B. Wilkinson, *Hypertension* **2008**, *51*, 1476.
[103] B. Williams, P. S. Lacy, S. M. Thom, K. Cruickshank, A. Stanton, D. Collier, A. D. Hughes, H. Thurston, M. O'Rourke, *Circulation* **2006**, *113*, 1213.
[104] Q. Zheng, H. Zhang, B. Shi, X. Xue, Z. Liu, Y. Jin, Y. Ma, Y. Zou, X. Wang, Z. An, W. Tang, W. Zhang, F. Yang, Y. Liu, X. Lang, Z. Xu, Z. Li, Z. L. Wang, *ACS Nano* **2016**, *10*, 6510.
[105] F. M. Rijnberg, M. G. Hazekamp, J. J. Wentzel, P. J. H. de Koning, J. J. M. Westenberg, M. R. M. Jongbloed, N. A. Blom, A. A. W. Roest, *Circulation* **2018**, *137*, 2393.
[106] R. C. Webb, Y. Ma, S. Krishnan, Y. Li, S. Yoon, X. Guo, X. Feng, Y. Shi, M. Seidel, N. H. Cho, J. Kurniawan, J. Ahad, N. Sheth, J. Kim, J. G. Taylor, T. Darlington, K. Chang, W. Huang, J. Ayers, A. Gruebele, R. M. Pielak, M. J. Slepian, Y. Huang, A. M. Gorbach, J. A. Rogers, *Sci. Adv.* **2015**, *1*, e1500701.
[107] J. Viventi, D.-H. Kim, J. D. Moss, Y.-S. Kim, J. A. Blanco, N. Annetta, A. Hicks, J. Xiao, Y. Huang, D. J. Callans, J. A. Rogers, B. Litt, *Sci. Transl. Med.* **2010**, *2*, 24ra22.
[108] D.-H. Kim, R. Ghaffari, N. Lu, S. Wang, S. P. Lee, H. Keum, R. D'Angelo, L. Klinker, Y. Su, C. Lu, Y.-S. Kim, A. Ameen, Y. Li, Y. Zhang, B. de Graff, Y.-Y. Hsu, Z. Liu, J. Ruskin, L. Xu, C. Lu, F. G. Omenetto, Y. Huang, M. Mansour, M. J. Slepian, J. A. Rogers, *Proc. Natl. Acad. Sci. USA* **2012**, *109*, 19910.
[109] S. Lee, Y. Inoue, D. Kim, A. Reuveny, K. Kuribara, T. Yokota, J. Reeder, M. Sekino, T. Sekitani, Y. Abe, T. Someya, *Nat. Commun.* **2014**, *5*, 5898.
[110] L. Xu, S. R. Gutbrod, A. P. Bonifas, Y. Su, M. S. Sulkin, N. Lu, H.-J. Chung, K.-I. Jang, Z. Liu, M. Ying, C. Lu, R. C. Webb, J.-S. Kim, J. I. Laughner, H. Cheng, Y. Liu, A. Ameen, J.-W. Jeong, G.-T. Kim, Y. Huang, I. R. Efimov, J. A. Rogers, *Nat. Commun.* **2014**, *5*, 3329.
[111] S. Choi, S. I. Han, D. Jung, H. J. Hwang, C. Lim, S. Bae, O. K. Park, C. M. Tschabrunn, M. Lee, S. Y. Bae, J. W. Yu, J. H. Ryu, S.-W. Lee,

K. Park, P. M. Kang, W. B. Lee, R. Nezafat, T. Hyeon, D.-H. Kim, *Nat. Nanotechnol.* **2018**, *13*, 1048.
[112] E. Cingolani, J. I. Goldhaber, E. Marban, *Nat. Rev. Cardiol.* **2018**, *15*, 139.
[113] C. A. Conde, J. Leppo, J. Lipski, B. Stimmel, R. Ltwak, E. Donoso, S. Dack, *Am. J. Cardiol.* **1973**, *32*, 209.
[114] M. R. Sohail, C. A. Henrikson, M. J. Braid-Forbes, K. F. Forbes, D. J. Lerner, *Arch. Intern. Med.* **2011**, *171*, 1821.
[115] A. Habib, K. Y. Le, L. M. Baddour, P. A. Friedman, D. L. Hayes, C. M. Lohse, W. R. Wilson, J. M. Steckelberg, M. R. Sohail, *Am. J. Cardiol.* **2013**, *111*, 874.
[116] S. K. Mulpuru, V. G. Pretorius, U. M. Birgersdotter-Green, *Circulation* **2013**, *128*, 1031.
[117] J. C. Nielsen, J. C. Gerdes, N. Varma, *Eur. Heart J.* **2015**, *36*, 2484.
[118] D. H. Lee, E. J. Gracely, S. Y. Aleem, S. P. Kutalek, O. Vielemeyer, *Pacing Clin. Electrophysiol.* **2015**, *38*, 1456.
[119] I. Diemberger, F. Migliore, M. Biffi, A. Cipriani, E. Bertaglia, S. Lorenzetti, G. Massaro, G. Tanzarella, G. Boriani, *Int. J. Cardiol.* **2018**, *250*, 146.
[120] C. R. Ellis, M. J. Kolek, *Comb. Prod. Ther.* **2011**, *1*, 003.
[121] H. L. Bloom, L. Constantin, D. Dan, D. B. De Lurgio, M. El-Chami, L. I. Ganz, K. J. Gleed, F. K. Hackett, N. K. Kanuru, D. J. Lerner, A. Rasekh, G. R. Simons, F. O. Sogade, M. R. Sohail, *Pacing Clin. Electrophysiol.* **2011**, *34*, 133.
[122] M. J. Kolek, W. F. Dresen, Q. S. Wells, C. R. Ellis, *Pacing Clin. Electrophysiol.* **2013**, *36*, 354.
[123] S. Mittal, R. E. Shaw, K. Michel, R. Palekar, A. Arshad, D. Musat, M. Preminger, T. Sichrovsky, J. S. Steinberg, *Heart Rhythm* **2014**, *11*, 595.
[124] N. Shariff, E. Eby, E. Adelstein, S. Jain, A. Shalaby, S. Saba, N. C. Wang, D. Schwartzman, *J. Cardiovasc. Electrophysiol.* **2015**, *26*, 783.
[125] M. J. Kolek, N. J. Patel, W. K. Clair, S. P. Whalen, J. N. Rottman, A. Kanagasundram, S. T. Shen, P. J. Saavedra, J. C. Estrada, R. L. Abraham, C. R. Ellis, *J. Cardiovasc. Electrophysiol.* **2015**, *26*, 1111.
[126] K. G. Tarakji, C. R. Ellis, P. Defaye, C. Kennergren, *Arrhythmia Electrophysiol. Rev.* **2016**, *5*, 65.
[127] G. Kay, E. L. Eby, B. Brown, J. Lyon, S. Eggington, G. Kumar, E. Fenwick, M. R. Sohail, D. J. Wright, *J. Med. Eco* **2018**, *21*, 294.
[128] C. A. Henrikson, M. R. Sohail, H. Acosta, E. E. Johnson, L. Rosenthal, R. Pachulski, D. Dan, W. Paladino, F. S. Khairallah, K. Gleed, I. Hanna, A. Cheng, D. R. Lexcen, G. R. Simons, *JACC: Clin. Electrophysiol.* **2017**, *3*, 1158.
[129] S. Ali, Y. Kanjwal, S. R. Bruhl, M. Alo, M. Taleb, S. S. Ali, A. Kabour, O. Khawaja, *Ther. Adv. Infect. Dis.* **2017**, *4*, 75.
[130] J. Thimot, K. L. Shepard, *Nat. Biomed. Eng.* **2017**, *1*, 0051.
[131] Q. Zheng, B. Shi, F. Fan, X. Wang, L. Yan, W. Yuan, S. Wang, H. Liu, Z. Li, Z. L. Wang, *Adv. Mater.* **2014**, *26*, 5851.
[132] W. Seung, M. K. Gupta, K. Y. Lee, K.-S. Shin, J.-H. Lee, T. Y. Kim, S. Kim, J. Lin, J. H. Kim, S.-W. Kim, *ACS Nano* **2015**, *9*, 3501.
[133] W. Tang, J. Tian, Q. Zheng, L. Yan, J. Wang, Z. Li, Z. L. Wang, *ACS Nano* **2015**, *9*, 7867.
[134] S. S. Kwak, H. Kim, W. Seung, J. Kim, R. Hinchet, S.-W. Kim, *ACS Nano* **2017**, *11*, 10733.
[135] S. Jung, J. Lee, T. Hyeon, M. Lee, D.-H. Kim, *Adv. Mater.* **2014**, *26*, 6329.
[136] S. Hong, J. Lee, K. Do, M. Lee, J. H. Kim, S. Lee, D.-H. Kim, *Adv. Funct. Mater.* **2017**, *27*, 1704353.
[137] C. Dagdeviren, B. D. Yang, Y. Su, P. L. Tran, P. Joe, E. Anderson, J. Xia, V. Doraiswamy, B. Dehdashti, X. Feng, B. Lu, R. Poston, Z. Khalpey, R. Ghaffari, Y. Huang, M. J. Slepian, J. A. Rogers, *Proc. Natl. Acad. Sci. USA* **2014**, *111*, 1927.
[138] G.-T. Hwang, H. Park, J.-H. Lee, S. Oh, K.-I. Park, M. Byun, H. Park, G. Ahn, C. K. Jeong, K. No, H. Kwon, S.-G. Lee, B. Joung, K. J. Lee, *Adv. Mater.* **2014**, *26*, 4880.
[139] K.-I. Park, J. H. Son, G.-T. Hwang, C. K. Jeong, J. Ryu, M. Koo, I. Choi, S. H. Lee, M. Byun, Z. L. Wang, K. J. Lee, *Adv. Mater.* **2014**, *26*, 2514.
[140] Y. Qi, N. T. Jafferis, K. Lyons, C. M. Lee, H. Ahmad, M. C. McAlpine, *Nano Lett.* **2010**, *10*, 524.
[141] C. Dagdeviren, Y. Shi, P. Joe, R. Ghaffari, G. Balooch, K. Usgaonkar, O. Gur, P. L. Tran, J. R. Crosby, M. Meyer, Y. Su, R. Chad Webb, A. S. Tedesco, M. J. Slepian, Y. Huang, J. A. Rogers, *Nat. Mater.* **2015**, *14*, 728.
[142] B. Lu, Y. Chen, D. Ou, H. Chen, L. Diao, W. Zhang, J. Zheng, W. Ma, L. Sun, X. Feng, *Sci. Rep.* **2015**, *5*, 16065.
[143] K. Song, J. H. Han, T. Lim, N. Kim, S. Shin, J. Kim, H. Choo, S. Jeong, Y.-C. Kim, Z. L. Wang, J. Lee, *Adv. Healthcare Mater.* **2016**, *5*, 1572.
[144] L. Bereuter, S. Williner, F. Pianezzi, B. Bissig, S. Buecheler, J. Burger, R. Vogel, A. Zurbuchen, A. Haeberlin, *Ann. Biomed. Eng.* **2017**, *45*, 1172.
[145] K. Song, J. H. Han, H. C. Yang, K. I. Nam, J. Lee, *Biosens. Bioelectron.* **2017**, *92*, 364.
[146] S. Burks, J. P. Kolcun, M. Y. Wang, *Neurosurgery* **2017**, *81*, N24.
[147] W. Lee, J. Lee, H. Yun, J. Kim, J. Park, C. Choi, D. C. Kim, H. Seo, H. Lee, J. W. Yu, W. B. Lee, D.-H. Kim, *Adv. Mater.* **2017**, *29*, 1702902.
[148] S. Xu, Y. Zhang, J. Cho, J. Lee, X. Huang, L. Jia, J. A. Fan, Y. Su, J. Su, H. Zhang, H. Cheng, B. Lu, C. Yu, C. Chuang, T.-I. Kim, T. Song, K. Shigeta, S. Kang, C. Dagdeviren, I. Petrov, P. V. Braun, Y. Huang, U. Paik, J. A. Rogers, *Nat. Commun.* **2013**, *4*, 1543.
[149] D. R. Agrawal, Y. Tanabe, D. Weng, A. Ma, S. Hsu, S.-Y. Liao, Z. Zhen, Z.-Y. Zhu, C. Sun, Z. Dong, F. Yang, H. F. Tse, A. S. Y. Poon, J. S. Ho, *Nat. Biomed. Eng.* **2017**, *1*, 0043.
[150] J. S. Ho, A. J. Yeh, E. Neofytou, S. Kim, Y. Tanabe, B. Patlolla, R. E. Beygui, A. S. Poon, *Proc. Natl. Acad. Sci. USA* **2014**, *111*, 7974.
[151] J. Kim, R. Ghaffari, D.-H. Kim, *Nat. Biomed. Eng.* **2017**, *1*, 0049.
[152] M. A. P. Mahmud, N. Huda, S. H. Farjana, M. Asadnia, C. Lang, *Adv. Energy Mater.* **2018**, *8*, 1701210.
[153] F. R. Fan, W. Tang, Z. L. Wang, *Adv. Mater.* **2016**, *28*, 4283.
[154] J. Briscoe, S. Dunn, *Nano Energy* **2015**, *14*, 15.
[155] R. Hinchet, S.-W. Kim, *ACS Nano* **2015**, *9*, 7742.
[156] S. H. Lee, C. K. Jeong, G.-T. Hwang, K. J. Lee, *Nano Energy* **2015**, *14*, 111.
[157] F.-R. Fan, Z.-Q. Tian, Z. L. Wang, *Nano Energy* **2012**, *1*, 328.
[158] H. L. Zhang, T. Van Gerven, J. Baeyens, J. Degreve, *Sci. World J.* **2014**, *2014*, 404913.
[159] G. Nichol, M. R. Sayre, F. Guerra, J. Poole, *J. Am. Coll. Cardiol.* **2017**, *70*, 1496.
[160] L. Xu, S. R. Gutbrod, Y. Ma, A. Petrossians, Y. Liu, R. C. Webb, J. A. Fan, Z. Yang, R. Xu, J. J. Whalen, J. D. Weiland, Y. Huang, I. R. Efimov, J. A. Rogers, *Adv. Mater.* **2015**, *27*, 1731.
[161] L. E. Rodriguez, E. E. Suarez, M. Loebe, B. A. Bruckner, *Methodist DeBakey Cardiovasc. J.* **2013**, *9*, 32.
[162] M. Kopernik, *Adv. Eng. Mater.* **2015**, *17*, 278.
[163] M. Kopernik, S. Kąc, M. Gawlikowski, G. Cios, *Adv. Eng. Mater.* **2016**, *18*, 795.
[164] M. M. Givertz, *Circulation* **2011**, *124*, e305.
[165] A. Zittermann, J. B. Ernst, S. Pilz, J. Dreier, J. Kuhn, C. Knabbe, J. F. Gummert, M. Morshuis, H. Milting, *PLoS One* **2016**, *11*, e0164459.
[166] B. Y. Chang, S. P. Keller, S. S. Bhavsar, N. Josephy, E. R. Edelman, *Sci. Transl. Med.* **2018**, *10*, eaao2980.
[167] M. C. Alraies, P. Eckman, *J. Thorac. Dis.* **2014**, *6*, 1120.
[168] V. Racca, P. Castiglioni, C. Panzarino, M. Saresella, I. Marventano, A. Verde, F. Oliva, M. Ferratini, *Sci. Rep.* **2018**, *8*, 10816.
[169] E. M. Schumer, M. C. Black, G. Monreal, M. S. Slaughter, *Eur. Heart J.* **2016**, *37*, 3434.

[170] J. Vierecke, M. Schweiger, D. Feldman, E. Potapov, F. Kaufmann, L. Germinario, R. Hetzer, V. Falk, T. Krabatsch, *Emerg. Med. J.* **2017**, *34*, 831.
[171] J. R. Reis Filho, J. N. Cardoso, C. M. Cardoso, A. C. Pereira-Barretto, *Arq. Bras. Cardiol.* **2015**, *104*, 502.
[172] B. Pieske, *Eur. Heart J. Suppl.* **2004**, *6*, D66.
[173] D. Burkhoff, S. Klotz, D. M. Mancini, *J. Card. Failure* **2006**, *12*, 227.
[174] A. V. Ambardekar, P. M. Buttrick, *Circ.: Heart Failure* **2011**, *4*, 224.
[175] M. C. Oz, J. H. Artrip, D. Burkhoff, *J. Heart Lung Transplant.* **2002**, *21*, 1049.
[176] W.-T. Wu, F. Yang, J. Wu, N. Aubry, M. Massoudi, J. F. Antaki, *Sci. Rep.* **2016**, *6*, 38025.
[177] W. F. Saavedra, R. S. Tunin, N. Paolocci, T. Mishima, G. Suzuki, C. W. Emala, P. A. Chaudhry, P. Anagnostopoulos, R. C. Gupta, H. N. Sabbah, D. A. Kass, *J. Am. Coll. Cardiol.* **2002**, *39*, 2069.
[178] C.-S. Jhun, N. Gundiah, K. Sun, H. N. Sabbah, E. E. Tseng, M. B. Ratcliffe, J. M. Guccione, in *Computational Cardiovascular Mechanics: Modelling and Applications in Heart Failure* (Eds: J. M. Guccione, G. S. Kassab, M. B. Ratcliffe), Springer US, New York, USA **2010**, Ch. 13.
[179] C. T. Klodell, J. M. Aranda, D. C. McGiffin, B. K. Rayburn, B. Sun, W. T. Abraham, W. E. Pae, J. P. Boehmer, H. Klein, C. Huth, *J. Thorac. Cardiovasc. Surg.* **2008**, *135*, 188.
[180] C. T. Klodell, D. C. McGiffin, B. K. Rayburn, B. Sun, W. T. Abraham, J. V. Conte, S. D. Russell, W. E. Pae, J. P. Boehmer, J. M. Aranda, *J. Thorac. and Cardiovasc. Surg.* **2007**, *133*, 204.
[181] J. A. Magovern, *Semin. Thorac. Cardiovasc. Surg.* **2005**, *17*, 364.
[182] L. S. Lee, R. K. Ghanta, S. A. Mokashi, O. Coelho-Filho, R. Y. Kwong, R. M. Bolman, F. Y. Chen, *J. Thorac. and Cardiovasc. Surg.* **2010**, *139*, 1012.
[183] R. K. Ghanta, A. Rangaraj, R. Umakanthan, L. Lee, R. G. Laurence, J. A. Fox, R. M. Bolman, L. H. Cohn, F. Y. Chen, *Circulation* **2007**, *115*, 1201.
[184] M. H. Kwon, M. Cevasco, J. D. Schmitto, F. Y. Chen, *J. Thorac. and Cardiovasc. Surg.* **2012**, *144*, 771.
[185] C. J. Payne, I. Wamala, C. Abah, T. Thalhofer, M. Saeed, D. Bautista-Salinas, M. A. Horvath, N. V. Vasilyev, E. T. Roche, F. A. Pigula, C. J. Walsh, *Soft Rob.* **2017**, *4*, 241.
[186] N. Lu, D.-H. Kim, *Soft Rob.* **2014**, *1*, 53.
[187] E. T. Roche, M. A. Horvath, I. Wamala, A. Alazmani, S.-E. Song, W. Whyte, Z. Machaidze, C. J. Payne, J. C. Weaver, G. Fishbein, J. Kuebler, N. V. Vasilyev, D. J. Mooney, F. A. Pigula, C. J. Walsh, *Sci. Transl. Med.* **2017**, *9*, eaaf3925.
[188] J. C. Criscione, *Nat. Biomed. Eng.* **2017**, *1*, 0046.
[189] E. T. Roche, R. Wohlfarth, J. T. Overvelde, N. V. Vasilyev, F. A. Pigula, D. J. Mooney, K. Bertoldi, C. J. Walsh, *Adv. Mater.* **2014**, *26*, 1200.
[190] I. Fernandez-Ruiz, *Nat. Rev. Cardiol.* **2017**, *14*, 129.
[191] E. T. Roche, M. A. Horvath, A. A. Nodeh, K. C. Galloway, N. V. Vasilyev, D. J. Mooney, F. A. Pigula, C. J. Walsh, presented at *Proc. ASME 2015 Int. Des. Eng. Tech. Conf. Comput. Inf. Eng. Conf.*, Boston, MA, USA, August **2015**.
[192] M. A. Horvath, E. T. Roche, D. M. Vogt, D. J. Mooney, F. A. Pigula, C. J. Walsh, presented at *Proc. ASME 2015 Int. Des. Eng. Tech. Conf. Comput. Inf. Eng. Conf.*, Boston, MA, USA, August **2015**.
[193] M. A. Horvath, C. E. Varela, E. B. Dolan, W. Whyte, D. S. Monahan, C. J. Payne, I. A. Wamala, N. V. Vasilyev, F. A. Pigula, D. J. Mooney, C. J. Walsh, G. P. Duffy, E. T. Roche, *Ann. Biomed. Eng.* **2018**, *46*, 1534.
[194] M. Naveed, L. Han, G. J. Khan, S. Yasmeen, R. Mikrani, M. Abbas, L. Cunyu, Z. Xiaohui, *Biomed. Pharmacother.* **2018**, *102*, 41.
[195] M. R. Moreno, S. Biswas, L. D. Harrison, G. Pernelle, M. W. Niller, T. W. Fossum, D. A. Nelson, J. C. Criscione, *J. Med. Devices* **2011**, *5*, 041008.
[196] M. R. Moreno, S. Biswas, L. D. Harrison, G. Pernelle, M. W. Miller, T. W. Fossum, D. A. Nelson, J. C. Criscione, *J. Med. Devices* **2011**, *5*, 041007.
[197] C. R. Greyson, *Crit. Care Med.* **2008**, *36*, S57.
[198] C. J. Payne, I. Wamala, D. Bautista-Salinas, M. Saeed, D. V. Story, T. Thalhofer, M. A. Horvath, C. Abah, P. J. del Nido, C. J. Walsh, N. V. Vasilyev, *Sci. Rob.* **2017**, *2*, eaan6736.
[199] E. Park, N. Mehandru, T. L. Beltran, E. Kraus, D. Holland, P. Polygerinos, N. V. Vasilyev, C. Walsh, *J. Med. Devices* **2014**, *8*, 020908.
[200] L. Macle, S. Nattel, *Nat. Rev. Cardiol.* **2016**, *13*, 67.
[201] A. Verma, C. Y. Jiang, T. R. Betts, J. Chen, I. Deisenhofer, R. Mantovan, L. Macle, C. A. Morillo, W. Haverkamp, R. Weerasooriya, J. P. Albenque, S. Nardi, E. Menardi, P. Novak, P. Sanders, *N. Engl. J. Med.* **2015**, *372*, 1812.
[202] S. P. Lee, L. E. Klinker, L. Ptaszek, J. Work, C. Liu, F. Quivara, C. Webb, C. Dagdeviren, J. A. Wright, J. N. Ruskin, M. Slepian, Y. Huang, M. Mansour, J. A. Rogers, R. Ghaffari, *Proc. IEEE* **2015**, *103*, 682.
[203] K. H. Kuck, J. Brugada, A. Furnkranz, A. Metzner, F. Ouyang, K. R. Chun, A. Elvan, T. Arentz, K. Bestehorn, S. J. Pocock, J. P. Albenque, C. Tondo, *N. Engl. J. Med.* **2016**, *374*, 2235.
[204] K. R. J. Chun, J. Brugada, A. Elvan, L. Geller, M. Busch, A. Barrera, R. J. Schilling, M. R. Reynolds, R. B. Hokanson, R. Holbrook, B. Brown, M. Schluter, K. H. Kuck, *J. Am. Heart Assoc.* **2017**, *6*, e006043.
[205] K. H. Kuck, V. Y. Reddy, B. Schmidt, A. Natale, P. Neuzil, N. Saoudi, J. Kautzner, C. Herrera, G. Hindricks, P. Jais, H. Nakagawa, H. Lambert, D. C. Shah, *Heart Rhythm* **2012**, *9*, 18.
[206] S. R. Dukkipati, P. Neuzil, J. Kautzner, J. Petru, D. Wichterle, J. Skoda, R. Cihak, P. Peichl, A. D. Russo, G. Pelargonio, C. Tondo, A. Natale, V. Y. Reddy, *Heart Rhythm* **2012**, *9*, 919.
[207] J. Osca, O. Cano, A. Andres, P. Alonso, M. J. Sancho-Tello, J. Olague, *Rev. Esp. Cardiol.* **2014**, *67*, 1061.
[208] S. R. Dukkipati, F. Cuoco, I. Kutinsky, A. Aryana, T. D. Bahnson, D. Lakkireddy, I. Woollett, Z. F. Issa, A. Natale, V. Y. Reddy, *J. Am. Coll. Cardiol.* **2015**, *66*, 1350.
[209] D.-H. Kim, N. Lu, R. Ghaffari, Y.-S. Kim, S. P. Lee, L. Xu, J. Wu, R.-H. Kim, J. Song, Z. Liu, J. Viventi, B. de Graff, B. Elolampi, M. Mansour, M. J. Slepian, S. Hwang, J. D. Moss, S.-M. Won, Y. Huang, B. Litt, J. A. Rogers, *Nat. Mater.* **2011**, *10*, 316.
[210] J. Kautzner, P. Neuzil, H. Lambert, P. Peichl, J. Petru, R. Cihak, J. Skoda, D. Wichterle, E. Wissner, A. Yulzari, K.-H. Kuck, *Europace* **2015**, *17*, 1229.
[211] V. Y. Reddy, D. Shah, J. Kautzner, B. Schmidt, N. Saoudi, C. Herrera, P. Jais, G. Hindricks, P. Peichl, A. Yulzari, H. Lambert, P. Neuzil, A. Natale, K. H. Kuck, *Heart Rhythm* **2012**, *9*, 1789.
[212] L. Klinker, S. Lee, J. Work, J. Wright, Y. Ma, L. Ptaszek, R. C. Webb, C. Liu, N. Sheth, M. Mansour, J. A. Rogers, Y. Huang, H. Chen, R. Ghaffari, *Extreme Mech. Lett.* **2015**, *3*, 45.
[213] A. Koh, S. R. Gutbrod, J. D. Meyers, C. Lu, R. C. Webb, G. Shin, Y. Li, S. K. Kang, Y. Huang, I. R. Efimov, J. A. Rogers, *Adv. Healthcare Mater.* **2016**, *5*, 373.
[214] Y. Su, Z. Liu, S. Wang, R. Ghaffari, D.-H. Kim, K.-C. Hwang, J. A. Rogers, Y. Huang, *Int. J. Solids Struct.* **2014**, *51*, 1555.
[215] H. Kottkamp, F. Moser, A. Riegr, D. Schreiber, C. Pönisch, M. Trofin, *J. Cardiovasc. Electrophysiol.* **2017**, *28*, 1247.
[216] A. Gruntzig, *Lancet* **1978**, *311*, 263.
[217] C. Landau, R. A. Lange, L. D. Hillis, *N. Engl. J. Med.* **1994**, *330*, 981.
[218] M. Nobuyoshi, T. Kimura, H. Nosaka, S. Mioka, K. Ueno, H. Yokoi, N. Hamasaki, H. Horiuchi, H. Ohishi, *J. Am. Coll. Cardiol.* **1988**, *12*, 616.
[219] P. Saraswat, M. Chinnakonda, B. Baillargeon, *J. Med. Devices* **2016**, *10*, 030945.

[220] E. Regar, G. Sianos, P. W. Serruys, *Br. Med. Bull.* **2001**, *59*, 227.
[221] T. Kimura, H. Yokoi, Y. Nakagawa, T. Tamura, S. Kaburagi, Y. Sawada, Y. Sato, H. Yokoi, N. Hamasaki, H. Nosaka, M. Nobuyoshi, *N. Engl. J. Med.* **1996**, *334*, 561.
[222] R. Waksman, A. Steinvil, *Cirs.: Cardiovasc. Intervention* **2016**, *9*, e004150.
[223] K. M. Lekshmi, H.-L. Che, C.-S. Cho, I.-K. Park, *Chonnam Med. J.* **2017**, *53*, 14.
[224] G. G. Stefanini, D. R. Holmes, *N. Engl. J. Med.* **2013**, *368*, 254.
[225] A. Dalmoro, A. A. Barba, M. Grassi, G. Grassi, G. Lamberti, *J. Biomed. Mater. Res., Part B* **2016**, *104*, 1013.
[226] H. Jia, S.-Y. Gu, K. Chang, *Adv. Polym. Technol.* **2018**, *00*, 1.
[227] G. I. Peterson, A. V. Dobrynin, M. L. Becker, *Adv. Healthcare Mater.* **2017**, *6*, 1700694.
[228] A. Colombo, E. Karvouni, *Circulation* **2000**, *102*, 371.
[229] S. S. Venkatraman, L. P. Tan, J. F. D. Joso, Y. C. F. Boey, X. Wang, *Biomaterials* **2006**, *27*, 1573.
[230] H. Hermawan, D. Dube, D. Mantovani, *Acta Biomater.* **2010**, *6*, 1693.
[231] S.-Y. Gu, K. Chang, S.-P. Jin, *J. Appl. Polym. Sci.* **2018**, *135*, 45686.
[232] P. Zartner, R. Cesnjevar, H. Singer, M. Weyand, *Catheterization Cardiovasc. Interventions* **2005**, *66*, 590.
[233] R. van Lith, E. Baker, H. Ware, J. Yang, A. C. Farsheed, C. Sun, G. Ameer, *Adv. Mater. Technol.* **2016**, *1*, 1600138.
[234] D. H. Keum, J. H. Mun, B. W. Hwang, J. Kim, H. Kim, W. Jo, D.-H. Ha, D.-W. Cho, C. Kim, S. K. Hahn, *Small* **2017**, *13*, 1602925.
[235] X. Chen, D. Brox, B. Assadsangabi, Y. Hsiang, K. Takahata, *Biomed. Microdevices* **2014**, *16*, 745.
[236] J. Park, J.-K. Kim, S. J. Patil, J.-K. Park, S. Park, D.-W. Lee, *Sensors* **2016**, *16*, 809.
[237] A. Viswanath, S. R. Green, J. Kosel, Y. B. Gianchandani, *J. Micromech. Microeng.* **2013**, *23*, 025010.
[238] X. Chen, B. Assadsangabi, Y. Hsiang, K. Takahata, *Adv. Sci.* **2018**, *5*, 1700560.
[239] D. Son, J. Lee, D. J. Lee, R. Ghaffari, S. Yun, S. J. Kim, J. E. Lee, H. R. Cho, S. Yoon, S. Yang, S. Lee, S. Qiao, D. Ling, S. Shin, J.-K. Song, J. Kim, T. Kim, H.-J. Lee, J. Kim, M. Soh, N. Lee, C. S. Hwang, S. Nam, N. Lu, T. Hyeon, S. H. Choi, D.-H. Kim, *ACS Nano* **2015**, *9*, 5937.
[240] H. Lee, C. Song, S. Baik, D. Kim, T. Hyeon, D.-H. Kim, *Adv. Drug Delivery Rev.* **2018**, *127*, 35.
[241] J. Park, J.-K. Kim, S. A. Park, D. S. Sim, M. H. Jeong, D.-W. Lee, presented at *19th Int. Conf. Solid-State Sensors, Actuators and Microsystems*, Kaohsiung, Taiwan, June **2017**.
[242] Y. Luo, M. Dahmardeh, X. Chen, K. Takahata, *Sens. Actuators, A* **2015**, *236*, 323.
[243] A. P. Beltrami, L. Barlucchi, D. Torella, M. Baker, F. Limana, S. Chimenti, H. Kasahara, M. Rota, E. Musso, K. Urbanek, A. Leri, J. Kajstura, B. Nadal-Ginard, P. Anversa, *Cell* **2003**, *114*, 763.
[244] B. E. Strauer, M. Brehm, T. Zeus, M. Köstering, A. Hernandez, R. V. Sorg, G. Kögler, P. Wernet, *Circulation* **2002**, *106*, 1913.
[245] C. Benden, S. B. Goldfarb, L. B. Edwards, A. Y. Kucheryavaya, J. D. Christie, A. I. Dipchand, F. Dobbels, B. J. Levvey, L. H. Lund, B. Meiser, R. D. Yusen, J. Stehlik, *J. Heart Lung Transplant.* **2014**, *33*, 1025.
[246] B. Gridelli, G. Remuzzi, *N. Engl. J. Med.* **2000**, *343*, 404.
[247] T. Wittwer, T. Wahlers, *Transplant Int.* **2008**, *21*, 113.
[248] C. Hengstenberg, M. L. Rose, E. G. J. Olsen, B. Maisch, *Eur. Heart J.* **1991**, *12*, 144.
[249] S. Toldo, M. Quader, F. N. Salloum, E. Mezzaroma, A. Abbate, *Int. J. Mol. Sci.* **2016**, *17*, 958.
[250] Y. S. Zhang, J. Aleman, A. Arneri, S. Bersini, F. Piraino, S. R. Shin, M. R. Dokmeci, A. Khademhosseini, *Biomed. Mater.* **2015**, *10*, 034006.
[251] A. Ghiroldi, M. Piccoli, F. Cirillo, M. M. Monasky, G. Ciconte, C. Pappone, L. Anastasia, *Int. J. Mol. Sci.* **2018**, *19*, 3194.
[252] V. F. M. Segers, R. T. Lee, *Nature* **2008**, *451*, 937.
[253] P. Menasche, *Nat. Rev. Cardiol.* **2018**, *15*, 659.
[254] M. Yanamandala, W. Zhu, D. J. Garry, T. J. Kamp, J. M. Hare, H. W. Jun, Y. S. Yoon, N. Bursac, S. D. Prabhu, G. W. Dorn, R. Bolli, R. N. Kitsis, J. Zhang, *J. Am. Coll. Cardiol.* **2017**, *70*, 766.
[255] M. Yousef, C. M. Schannwell, M. Kostering, T. Zeus, M. Brehm, B. E. Strauer, *J. Am. Coll. Cardiol.* **2009**, *53*, 2262.
[256] H. Hashimoto, E. N. Olson, R. Bassel-Duby, *Nat. Rev. Cardiol.* **2018**, *15*, 585.
[257] R. de Jong, J. H. Houtgraaf, S. Samiei, E. Boersma, H. J. Duckers, *Circ.: Cardiovasc. Interventions* **2014**, *7*, 156.
[258] J. Bartunek, M. Vanderheyden, B. Vandekerckhove, S. Mansour, B. De Bruyne, P. De Bondt, I. Van Haute, N. Lootens, G. Heyndrickx, W. Wijns, *Circulation* **2005**, *112*, I178.
[259] V. Schachinger, S. Erbs, A. Elsasser, W. Haberbosch, R. Hambrecht, H. Holschermann, J. Yu, R. Corti, D. G. Mathey, C. W. Hamm, T. Suselbeck, N. Werner, J. Haase, J. Neuzner, A. Germing, B. Mark, B. Assmus, T. Tonn, S. Dimmeler, A. M. Zeiher, *Eur. Heart J.* **2006**, *27*, 2775.
[260] C. Mao, X. Hou, B. Wang, J. Chi, Y. Jiang, C. Zhang, Z. Li, *Stem Cell Res. Ther.* **2017**, *8*, 18.
[261] S. Yue, M. Naveed, W. Gang, D. Chen, Z. Wang, F. Yu, X. Zhou, *Biomed. Microdevices* **2018**, *20*, 40.
[262] Y. Guo, M. Wysoczynski, Y. Nong, A. Tomlin, X. Zhu, A. M. Gumpert, M. Nasr, S. Muthusamy, H. Li, M. Book, A. Khan, K. U. Hong, Q. Li, R. Bolli, *Basic Res. Cardiol.* **2017**, *112*, 18.
[263] A. A. Mangi, N. Noiseux, D. Kong, H. He, M. Rezvani, J. S. Ingwall, V. J. Dzau, *Nat. Med.* **2003**, *9*, 1195.
[264] P. Korpisalo, H. Karvinen, T. T. Rissanen, J. Kilpijoki, V. Marjomaki, P. Baluk, D. M. McDonald, Y. Cao, U. Eriksson, K. Alitalo, S. Yla-Herttuala, *Circ. Res.* **2008**, *103*, 1092.
[265] S. Zacchigna, V. Martinelli, S. Moimas, A. Colliva, M. Anzini, A. Nordio, A. Costa, M. Rehman, S. Vodret, C. Pierro, G. Colussi, L. Zentilin, M. I. Gutierrez, E. Dirkx, C. Long, G. Sinagra, D. Klatzmann, M. Giacca, *Nat. Commun.* **2018**, *9*, 2432.
[266] C. Stamm, B. Westphal, H.-D. Kleine, M. Petzsch, C. Kittner, H. Klinge, C. Schümichen, C. A. Nienaber, M. Freund, G. Steinhoff, *Lancet* **2003**, *361*, 45.
[267] T. Shimizu, M. Yamato, A. Kikuchi, T. Okano, *Biomaterials* **2003**, *24*, 2309.
[268] Y. Akiyama, A. Kikuchi, M. Yamato, T. Okano, *Langmuir* **2004**, *20*, 5506.
[269] Y. Miyahara, N. Nagaya, M. Kataoka, B. Yanagawa, K. Tanaka, H. Hao, K. Ishino, H. Ishida, T. Shimizu, K. Kangawa, S. Sano, T. Okano, S. Kitamura, H. Mori, *Nat. Med.* **2006**, *12*, 459.
[270] X. Zong, H. Bien, C.-Y. Chung, L. Yin, D. Fang, B. S. Hsiao, B. Chu, E. Entcheva, *Biomaterials* **2005**, *26*, 5330.
[271] J. H. Sung, M. L. Shuler, *Ann. Biomed. Eng.* **2012**, *40*, 1289.
[272] M. Radisic, H. Park, H. Shing, T. Consi, F. J. Schoen, R. Langer, L. E. Freed, G. Vunjak-Novakovic, *Proc. Natl. Acad. Sci. USA* **2004**, *101*, 18129.
[273] G. C. Engelmayr, M. Cheng, C. J. Bettinger, J. T. Borenstein, R. Langer, L. E. Freed, *Nat. Mater.* **2008**, *7*, 1003.
[274] Y. Wu, L. Wang, B. Guo, P. X. Ma, *ACS Nano* **2017**, *11*, 5646.
[275] S. Fleischer, A. Shapira, R. Feiner, T. Dvir, *Proc. Natl. Acad. Sci. USA* **2017**, *114*, 1898.
[276] J. L. Drury, D. J. Mooney, *Biomaterials* **2003**, *24*, 4337.
[277] B. Liu, B. W. Lee, K. Nakanishi, A. Villasante, R. Williamson, J. Metz, J. Kim, M. Kanai, L. Bi, K. Brown, G. Di Paolo, S. Homma, P. A. Sims, V. K. Topkara, G. Vunjak-Novakovic, *Nat. Biomed. Eng.* **2018**, *2*, 293.
[278] Y. Luo, M. S. Shoichet, *Nat. Mater.* **2004**, *3*, 249.

[279] Y. S. Kim, K. Cho, H. J. Lee, S. Chang, H. Lee, J. H. Kim, W.-G. Koh, *React. Funct. Polym.* **2016**, *109*, 15.
[280] S. Khorshidi, A. Karkhaneh, *J. Biomed. Mater. Res., Part A* **2018**, *106*, 718.
[281] J.-O. You, M. Rafat, G. J. Ye, D. T. Auguste, *Nano Lett.* **2011**, *11*, 3643.
[282] T. Dvir, B. P. Timko, M. D. Brigham, S. R. Naik, S. S. Karajanagi, O. Levy, H. Jin, K. K. Parker, R. Langer, D. S. Kohane, *Nat. Nanotechnol.* **2011**, *6*, 720.
[283] M. Montgomery, S. Ahadian, L. Davenport Huyer, M. Lo Rito, R. A. Civitarese, R. D. Vanderlaan, J. Wu, L. A. Reis, A. Momen, S. Akbari, A. Pahnke, R.-K. Li, C. A. Caldarone, M. Radisic, *Nat. Mater.* **2017**, *16*, 1038.
[284] A. A. Kocher, M. D. Schuster, M. J. Szabolcs, S. Takuma, D. Burkhoff, J. Wang, S. Homma, N. M. Edwards, S. Itescu, *Nat. Med.* **2001**, *7*, 430.
[285] M. Lovett, K. Lee, A. Edwards, D. L. Kaplan, *Tissue Eng., Part B* **2009**, *15*, 353.
[286] H. Bramfeldt, G. Sabra, V. Centis, P. Vermette, *Curr. Med. Chem.* **2010**, *17*, 3944.
[287] M. W. Laschke, A. Strohe, C. Scheuer, D. Eglin, S. Verrier, M. Alini, T. Pohlemann, M. D. Menger, *Acta Biomater.* **2009**, *5*, 1991.
[288] M. Shevach, N. Soffer-Tsur, S. Fleischer, A. Shapira, T. Dvir, *Biofabrication* **2014**, *6*, 024101.
[289] J. S. Miller, K. R. Stevens, M. T. Yang, B. M. Baker, D. H. Nguyen, D. M. Cohen, E. Toro, A. A. Chen, P. A. Galie, X. Yu, R. Chaturvedi, S. N. Bhatia, C. S. Chen, *Nat. Mater.* **2012**, *11*, 768.
[290] B. Zhang, M. Montgomery, M. D. Chamberlain, S. Ogawa, A. Korolj, A. Pahnke, L. A. Wells, S. Masse, J. Kim, L. Reis, A. Momen, S. S. Nunes, A. R. Wheeler, K. Nanthakumar, G. Keller, M. V. Sefton, M. Radisic, *Nat. Mater.* **2016**, *15*, 669.
[291] D. Iandolo, A. Ravichandran, X. Liu, F. Wen, J. K. Chan, M. Berggren, S.-H. Teoh, D. T. Simon, *Adv. Healthcare Mater.* **2016**, *5*, 1505.
[292] Z. Yan, M. Han, Y. Shi, A. Badea, Y. Yang, A. Kulkarni, E. Hanson, M. E. Kandel, X. Wen, F. Zhang, Y. Luo, Q. Lin, H. Zhang, X. Guo, Y. Huang, K. Nan, S. Jia, A. W. Oraham, M. B. Mevis, J. Lim, X. Guo, M. Gao, W. Ryu, K. J. Yu, B. G. Nicolau, A. Petronico, S. S. Rubakhin, J. Lou, P. M. Ajayan, K. Thornton, G. Popescu, D. Fang, J. V. Sweedler, P. V. Braun, H. Zhang, R. G. Nuzzo, Y. Huang, Y. Zhang, J. A. Rogers, *Proc. Natl. Acad. Sci. USA* **2017**, *114*, E9455.
[293] A. E. Jakus, E. B. Secor, A. L. Rutz, S. W. Jordan, M. C. Hersam, R. N. Shah, *ACS Nano* **2015**, *9*, 4636.
[294] W. Li, J. Wang, J. Ren, X. Qu, *Adv. Mater.* **2013**, *25*, 6737.
[295] L. H. Nguyen, M. Gao, J. Lin, W. Wu, J. Wang, S. Y. Chew, *Sci. Rep.* **2017**, *7*, 42212.
[296] B. Tian, J. Liu, T. Dvir, L. Jin, J. H. Tsui, Q. Qing, Z. Suo, R. Langer, D. S. Kohane, C. M. Lieber, *Nat. Mater.* **2012**, *11*, 986.
[297] J. Kim, W. A. Li, Y. Choi, S. A. Lewin, C. S. Verbeke, G. Dranoff, D. J. Mooney, *Nat. Biotechnol.* **2015**, *33*, 64.
[298] R. Feiner, L. Engel, S. Fleischer, M. Malki, I. Gal, A. Shapira, Y. Shacham-Diamand, T. Dvir, *Nat. Mater.* **2016**, *15*, 679.
[299] R. J. Wade, E. J. Bassin, C. B. Rodell, J. A. Burdick, *Nat. Commun.* **2015**, *6*, 6639.
[300] L. Yang, S. D. Chueng, Y. Li, M. Patel, C. Rathnam, G. Dey, L. Wang, L. Cai, K.-B. Lee, *Nat. Commun.* **2018**, *9*, 3147.
[301] D. Grafahrend, K.-H. Heffels, M. V. Beer, P. Gasteier, M. Moller, G. Boehm, P. D. Dalton, J. Groll, *Nat. Mater.* **2011**, *10*, 67.
[302] R. Feiner, S. Fleischer, A. Shapira, O. Kalish, T. Dvir, *J. Controlled Release* **2018**, *281*, 189.
[303] G. Bergstrom, J. Christoffersson, K. Schwanke, R. Zweigerdt, C.-F. Mandenius, *Lab Chip* **2015**, *15*, 3242.
[304] G. G. Giobbe, F. Michielin, C. Luni, S. Giulitti, S. Martewicz, S. Dupont, A. Floreani, N. Elvassore, *Nat. Methods* **2015**, *12*, 637.
[305] B. Zhang, A. Korolj, B. F. L. Lai, M. Radisic, *Nat. Rev. Mater.* **2018**, *3*, 257.
[306] X. Dai, W. Zhou, T. Gao, J. Liu, C. M. Lieber, *Nat. Nanotechnol.* **2016**, *11*, 776.
[307] V. Parpura, *Nat. Nanotechnol.* **2016**, *11*, 738.
[308] J. U. Lind, M. Yadid, I. Perkins, B. B. O'Connor, F. Eweje, C. O. Chantre, M. A. Hemphill, H. Yuan, P. H. Campbell, J. J. Vlassak, K. K. Parker, *Lab Chip* **2017**, *17*, 3692.
[309] J. U. Lind, T. A. Busbee, A. D. Valentine, F. S. Pasqualini, H. Yuan, M. Yadid, S. J. Park, A. Kotikian, A. P. Nesmith, P. H. Campbell, J. J. Vlassak, J. A. Lewis, K. K. Parker, *Nat. Mater.* **2017**, *16*, 303.